Chemical Geology 426 (2016) 1–18

Contents lists available at ScienceDirect

Chemical Geology

journal homepage: www.elsevier.com/locate/chemgeo

Solid-phase redistribution of rare earth elements in hillslope pedons subjected to different hydrologic fluxes

Angélica Vázquez-Ortega [a], David Huckle [b], Julia Perdrial [a,c], Mary Kay Amistadi [a], Matej Durcik [d], Craig Rasmussen [a], Jennifer McIntosh [b], Jon Chorover [a,*]

[a] Department of Soil, Water & Environmental Science, University of Arizona, 1177 East Fourth Street, Tucson, AZ 85721-0038, USA
[b] Department of Hydrology and Water Resources, University of Arizona, 1133 East James E. Rogers Way, Tucson, AZ 85721-0011, USA
[c] Department of Geology, University of Vermont, 180 Colchester Avenue, Burlington, VT 05401, USA
[d] Biosphere 2, University of Arizona, 845 North Park Avenue, Tucson, AZ 85721-0158, USA

ARTICLE INFO

Article history:
Received 30 September 2015
Received in revised form 30 December 2015
Accepted 1 January 2016
Available online 7 January 2016

Keywords:
Rare earth elements
Biological weathering
Critical zone
Pedogenesis
Mineral transformation

ABSTRACT

Prior studies indicate that patterns of rare earth element (REE) depletion or enrichment in critical zone (CZ) weathering systems are sensitive to variation not only in lithology, but also in climatic and/or biological processes. Organic ligands and secondary mineral surfaces vary in complex stability with different lanthanide series metals, which can result in solid-solution fractionation during incongruent mineral dissolution. REE fractionation during precipitation of solid phase weathering products is also expected to vary with host phase affinity and aqueous geochemistry along fluid flow paths. We postulated that patterns of REE fractionation during pedogenic weathering would exhibit mass-dependent trends as a function of depth in the soil profile. We further hypothesized that REE signatures would be influenced by depth-dependent variation in water and dissolved organic carbon (DOC) fluxes resulting from topographic position of the pedon under investigation. Field-based hypothesis testing utilized instrumented pedons derived from rhyolitic bedrock overlain by mixed conifer forest in the Jemez River Basin Critical Zone Observatory (JRB-CZO). REE depletion trends correlated with topographically-induced variation in soil pore water and DOC through-fluxes occurring predominantly during winter snowmelt. Bulk regolith analyses indicated that light rare earth elements (LREE) were depleted preferentially relative to medium and heavy REE (MREE and HREE). Lateral fluxes of water and DOC through subsurface horizons in the concave hillslope pedon correlated not only with greater REE depletion, but also with greater fractionation of REE into organo-metal colloid forms (2–23%) relative to a planar site hillslope pedon (3–13%) where vertical water and DOC fluxes were predominant. MREEs were preferentially retained in secondary colloids, indicating a mechanism for their stabilization in the weathering profile. Positive Ce-anomalies in the soils were the result of Ce retention in pedogenic Fe-(oxy)hydroxides.

1. Introduction

The lanthanide series of rare earth elements (REE, atomic numbers 53 through 71) is characterized by systematic variation in atomic mass, ionic radius, and electron configuration, as well as variation in oxidation state (Bau et al., 1995; Bau, 1999; Ohta and Kawabe, 2001; Davranche et al., 2004, 2011; Pourret et al., 2007b; Bau and Koschinsky, 2009). Fractionation behavior of the rare earth elements and yttrium (REY, the latter being included because of similar primary mineral sourcing and chemical reactivity as the lanthanides) has been used to elucidate soil and sediment biogeochemical weathering processes such as mineral dissolution, argilluviation, redox fluctuations, and biological cycling among others (Ronov et al., 1967; Cullers et al., 1975; Aubert et al., 2001, 2002; Coppin et al., 2002; Stille et al., 2006a, b, 2009; Nezat et al., 2007; Leybourne and Johannesson, 2008; Shiller, 2010; Tang and Johannesson, 2003, 2010a,b; Ma et al., 2011; Willis and Johannesson, 2011; Brioschi et al., 2013; Gangloff et al., 2014).

Systematic variation in chemical properties across the REY (e.g., the lanthanide contraction effect) (Sonke and Salters, 2006) leads to series wide trends in incorporation into (or exclusion from) secondary minerals and/or complexes with organic and inorganic ligands The variation also makes them appropriate for studies of biogeochemical weathering and fractionation during biogeochemical denudation of regolith (Elderfield, 1988; Elderfield et al., 1990; Wood, 1990; Sholkovitz,

Abbreviations: Ce/Ce*, cerium anomaly; CZ, critical zone; DOC, dissolved organic carbon; DOM, dissolved organic matter; Eu/Eu*, europium anomaly; HREE, heavy rare earth elements; JRB-CZO, Jemez River Basin Critical Zone Observatory; LREE, light rare earth elements; LRO, long range order; MC, mixed conifer; MREE, medium rare earth elements; OC, organic carbon; PCap, passive capillary sampler; REE, rare earth elements; REY, rare earth elements and yttrium; SE, sequential extraction; SOM, soil organic matter; SRO, short range order; TWI, topographic wetness index; UCC, upper continental crustal; WY, water years; ZOB, zero order basin.

* Corresponding author.
E-mail address: chorover@email.arizona.edu (J. Chorover).

http://dx.doi.org/10.1016/j.chemgeo.2016.01.001
0009-2541/

1992; Johannesson et al., 1997). Chemical reactions with soluble ligands, soil organic matter, layer silicate clays, Fe, Mn, and Al-(oxy)hydroxides, as well as variations in redox status have all been reported to influence REY fractionation, transport, and fate in soils and natural waters (Goldberg et al., 1963; Cullers et al., 1975; Viers et al., 1997; DeBaar et al., 1988; Elderfield, 1988; Nakajima and Terakado, 2003; Pourret et al., 2007b; Steinmann and Stille, 2008; Laveuf et al., 2008, 2012; Laveuf and Cornu, 2009; Goyne et al., 2010; Guo et al., 2010b; Johannesson et al., 2014).

The current study investigates partitioning of REY between mobile porewaters (predominantly snowmelt-derived) and residual soils originated from rhyolitic bedrock. We sought to evaluate the extent to which lanthanide series fractionation patterns, Y/Ho divergence, and Ce anomalies can be used to quantify the relative contributions of "biological weathering", as reflected in organic ligand-promoted REY fractionation between mobile fluids and weathering residuum. We postulated that 'bio-inorganic' solid phase products of similar lability (as measured by kinetic metal dissolution during sequential aqueous chemical extraction) will contain specific REY signatures denoting their pedogenic origin. In particular, we are interested in probing how REY signatures change as one moves from the complex of exchangeable cations, into organo-mineral colloids, and across a range of metal (oxy)hydroxide crystallinity. These same solid phase products form stable hetero-aggregates of mineral and organic matter. Therefore, it was of interest to determine whether mineral-stabilized organic matter with relatively long turnover times (e.g., see Torn et al., 1997; Mikutta et al., 2012) contains specific REY signatures. Thus, such signatures translocated episodically into surface waters could signal organic matter destabilization.

In the Jemez River Basin Critical Zone Observatory (JRB-CZO) infiltrating snowmelt transports a large seasonal pulse of soluble organic carbon through instrumented pedons (Perdrial et al., 2012, 2014a; Vázquez-Ortega et al., 2015). Infrared and fluorescence spectroscopy studies of the dissolved organic matter (DOM) in JRB-CZO soils indicated that they comprise a mixture of plant-derived polyphenols, as well as microbial polysaccharides and proteins, with the ratio of plant versus microbial fluorescent components showing seasonal and sorption–desorption dependence (Perdrial et al., 2014a; Vázquez-Ortega et al., 2014). We previously showed that total REY concentrations in effluent waters across a range of nested, instrumented catchment scales – hillslope to catchment to watershed – were strongly controlled by DOC concentration, and exhibited similar REY/DOC mass ratios (Vázquez-Ortega et al., 2015). Furthermore, soils distributed in different landscape positions contributing to catchment REY effluxes exhibited distinct depth-dependent chemical depletion patterns and an increase in the magnitude of positive Ce-anomalies with depth (preferential accumulation of Ce in deeper horizons with respect to host lithologies). Those results led to the further specific hypotheses tested in the current work: (i) REY depletion patterns reflect landscape-location-specific patterns of water and organic carbon flux observed at the sub-pedon scale; (ii) Ce is preferentially accumulated in lower horizons by adsorption and/or co-precipitation with Fe-(oxy)hydroxide minerals; and (iii) depth dependent trends in Y/Ho ratio reflect differential incorporation of these elements in pedogenic Fe-(oxy)hydroxide precipitates (e.g., Bau, 1999; Thompson et al., 2013) despite the fact that no systematic variations in Y/Ho ratios were observed in bulk soils.

As a result, the principal objective of the present study was to quantify mineral and organic phases controlling the retention of REY as a function of depth in pedons located in three distinct landscape positions (planar, convex, and concave) within a single zero order basin. A sequential chemical extraction procedure was performed to quantify the mass fraction of REY incorporated into adsorbed versus co-precipitated secondary species including Mn-oxides (e.g., birnessite), organo-metal colloids, short range order (SRO) Fe-oxides (e.g., ferrihydrite), long range order (LRO) Fe-oxides, (e.g., goethite), and residual materials (Land et al., 1999; Laveuf et al., 2012).

2. Materials and methods

2.1. Study site and sample collection

The study utilized data and samples obtained from six instrumented pedons under mixed conifer (MC) forest in a 0.15 km^2 zero order basin (ZOB) of the La Jara catchment that is part of the East Fork Jemez River watershed within the Valles Caldera National Preserve, NM (Fig. 1). The ZOB has a south-facing orientation with dominant SW and SE facing slopes separated by a concave swale that displays negligible surface flows outside of high discharge events and then only at the ZOB outlet (flume location, Fig. 1). The instrumented ZOB is the focus of inter-disciplinary surface earth process studies within the JRB-CZO (NRC, 2001; Brooks and Vivoni, 2008; Chorover et al., 2011; Vázquez-Ortega et al., 2015). Soils are established on Pleistocene aged rhyolitic volcaniclastic parent materials. Bedrock comprises a mixture of fine-grained porphyritic rhyodacite and hydrothermally altered Bandelier Tuff (http://geoinfo.nmt.edu/publications/maps/geologic/ofgm/). Parent materials were impacted by alkaline hydrothermal alteration soon after caldera collapse yielding transformation of volcanic glass dominantly to smectite with some zeolite (Goff and Gardner, 1988; Chipera et al., 2008). Outcrop samples of the parent rocks were collected in summer 2010 around Redondo Dome spanning the range of lithologic variation. Soils are derived from rhyolitic bedrock and tuff (Perdrial et al., 2012; Vázquez-Ortega et al., 2015). Soil solid samples were obtained from Pedon 1 (planar), Pedon 3 (convex), and Pedon 5 (concave) hillslope profiles, all excavated at the time of sampler installations (September, 2010). Soil samples were collected by genetic horizon, sealed in zip-lock bags and stored at 4 °C. Upon return to the lab, soil samples were air dried, sieved to recover the <2 mm fraction, homogenized, and stored at room temperature prior to further chemical analysis.

The six MC ZOB pedons were instrumented with in situ passive capillary soil solution (i.e., "PCap" or "wick") samplers that have been shown effective for REY and DOC pore water chemistry sampling (Holder et al., 1991; Biddle et al., 1995; Perdrial et al., 2012, 2014b) at 10, 30 and 60 cm depths. Flux values for DOC and REY were determined as the product of solution mass and molality for each sampling date, summing these products across all sampling dates per water year, and normalizing the result to the cross-sectional area of the wick sampler plate (0.09 m^2). Porewater samples were filtered through combusted 0.7 μm glass fiber filters (GF/F, Whatman, Alameda Chemical & Scientific Inc., Oakland, CA) for DOC and through 0.45 μm nylon filters (Millipore, Thermo Fisher Scientific) for metals, into separate acid washed HDPE bottles and transported under refrigerations (~4 °C) to the laboratory within a maximum of 2 d after sampling. All soil solutions included in this study were collected during the water years (WY) of 2011, 2012 and 2013. Water years are defined as October 1 to September 30.

2.2. Solid phase characterization

Bulk soil samples and parent materials (porphyritic rhyodacite and altered Bandelier Tuff) were analyzed for total elemental composition by lithium metaborate/tetraborate fusion followed dissolution of the pellet in nitric acid and solution phase analysis by inductively coupled plasma (ICP) optical emission spectrometry (-OES) and mass spectrometry (-MS) (Activation Laboratories, Ancaster, Ontario). Recovery of REY for certified standards W-2a (U.S. Geological Survey mafic rock reference) and NCS DC70009 (tungsten ore) were in the range of 95–105% and 94–104%, respectively. Total organic carbon in the bulk solid samples was determined by high temperature oxidation followed by infrared detection of CO_2 using a Shimadzu TOC-VCSH system equipped with a solid sample module SSM-5000A (Columbia, MD). Organic C, P, Mn, and Fe concentrations in bulk soil for the planar, convex, and concave hillslope profiles located in the La Jara ZOB are included in Table 1.

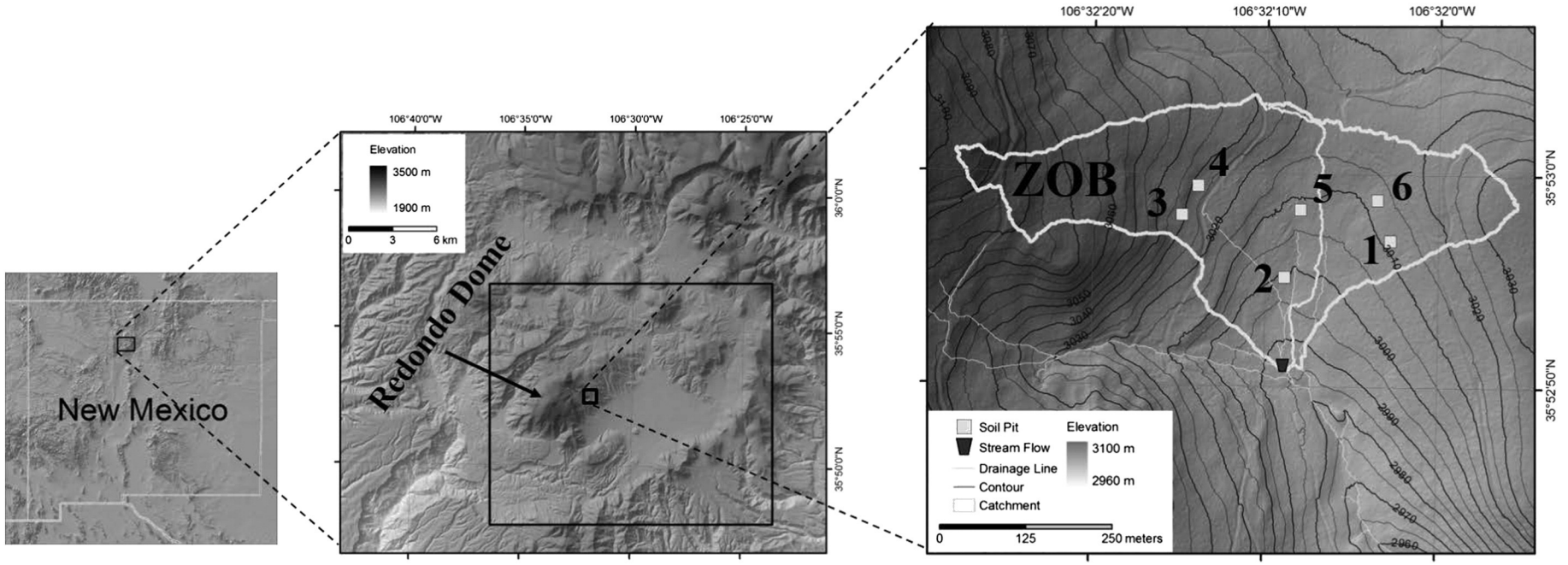

Fig. 1. New Mexico map (left panel) indicating the location of the study site in the Jemez Mountains. Valles Caldera National Preserve map including Redondo Dome (middle panel). Digital elevation model derived from CZO LiDAR data showing the instrumented pedons (numbered 1–6, installed in September 2010) located in La Jara Zero Order basin (ZOB) (right panel). The present study focuses on REY distribution specifically in Pedon 1 (planar hillslope location), Pedon 3 (convex hillslope location) and Pedon 5 (concave hillslope location) which exhibit topographically-induced variations in water and dissolved organic carbon fluxes that occur predominantly during winter snowmelt.

Table 1
Organic carbon (OC), P, Mn, and Fe concentrations (reported in g kg^{-1}) in the bulk soil for the planar, convex, and concave hillslope profiles located in the La Jara ZOB. Uncertainty values in parenthesis were calculated based on certified and measured values of standard NIST 694.

Location	Horizon	OC	P	Mn	Fe	Mn:Fe ratio
		(g kg^{-1})				
Planar	O	160 (30)	0.7 (7.0E−04)	3.81 (0.13)	13.4 (0.8)	1:05
	A	14 (3)	0.2 (2.0E−04)	1.27 (0.04)	12.8 (0.8)	1:16
	B1	3.1 (0.8)	0.09 (9.0E−05)	0.46 (0.02)	12.8 (0.8)	1:28
	B2	2.7 (0.5)	0.09 (9.0E−05)	0.41 (0.01)	15.0 (0.9)	1:67
	B3	2.2 (0.4)	0.1 (1.0E−04)	0.36 (0.01)	20.6 (1.3)	1:57
Convex	O	260 (40)	1.4 (1.4E−03)	0.84 (0.03)	12.3 (1.0)	1:17
	A	50 (7)	0.7 (7.0E−04)	0.84 (0.03)	18.4 (1.2)	1:19
	A/B	14 (2)	0.7 (7.0E−04)	1.01 (0.05)	18.0 (1.3)	1:14
	B1	8 (1)	0.5 (5.0E−04)	1.16 (0.04)	15.0 (1.3)	1:19
	B2	1.8 (0.3)	0.3 (3.0E−04)	0.46 (0.04)	16.4 (2.2)	1:29
Concave	O	230 (3)	1.4 (1.4E−03)	1.93 (0.07)	15.7 (1.0)	1:13
	A	52.5 (0.8)	0.7 (7.0E−04)	1.58 (0.05)	18.6 (1.2)	1:19
	B1	170 (3)	0.7 (7.0E−04)	1.57 (0.05)	20.8 (1.3)	1:14
	B2	190 (3)	0.5 (5.0E−04)	1.22 (0.04)	20.0 (1.3)	1:19
	B3	1.89 (0.03)	0.3 (3.0E−04)	1.21 (0.04)	35.5 (2.2)	1:29

According to X-ray diffraction (XRD) analysis, the mineralogical composition of rhyodacite includes predominantly albite ($NaAlSi_3O_8$), quartz (SiO_2), and sanidine ($(K,Na)(Si,Al)_4O_8$), whereas for tuff mineral composition is dominantly Ca-clinoptilolite ($CaAl_3(Al,Si)_2Si_{13}O_{36}\cdot 12H_2O$), sanidine, and cristobalite (polymorph of SiO_2). The crystalline mineralogical composition of the ZOB soils includes dominantly quartz, orthoclase ($KAlSi_3O_8$), muscovite ($KAl_2(Si_3Al)O_{10}(OH)_2$), oligoclase ($(Ca,Na)(Al,Si)_4O_8$), biotite ($K(Mg,Fe)_3AlSi_3O_{10}(OH)_2$), Ca-clinoptilolite, and kaolinite ($Al_2Si_2O_5(OH)_4$). More details on the physico-chemical characterization of the parent materials and ZOB soils are described in Vázquez-Ortega et al. (2015).

2.3. Landscape analysis

Topographic wetness index (TWI) and landscape curvature were calculated from LiDAR data to provide a quantitative description of pedon landscape position, and to enable interpretation of its impact on the local hydrologic and geochemical fluxes. TWI was calculated as $TWI = \ln(a / \tan\beta)$ (Beven and Kirkby, 1979), where a is the upslope contributing area in square meters and β is the local slope. The contributing area was calculated using the D-Infinity multiple flow direction approach as described by Tarboton (1997). Profile, plan and combined curvatures were calculated using the ArcGIS 10.2 3D Analyst tool. Combined curvature was computed as the second derivative of the surface elevation for each cell using eight surrounding cells. Profile curvature in the direction of the maximum slope represents the rate of change of slope, which influences erosion and deposition through the acceleration and deceleration of flow. The plan curvature is perpendicular to the direction of maximum slope and influences the convergence and divergence of flow across a surface (Zevenbergen and Thorne, 1987; Moore et al., 1991). For the plan and combined curvature outputs, a positive curvature indicates the surface is upwardly convex at that position, whereas a negative curvature indicates the surface is upwardly concave. A value of 0 indicates the surface is planar in all curvature approaches (Table A.1). The TWI and curvature were computed using a 1 m LiDAR dataset (Guo et al., 2010a) up-scaled to 10 m to smooth the uneven surface generated from the LiDAR scan while preserving principal topographic features in the ZOB.

2.4. Sequential chemical extractions

Soil samples were subjected to a five-step sequential extraction (SE) scheme (adapted from Land et al., 1999 and Laveuf et al., 2012) as summarized in Table 2. Extractions were performed in triplicate on 1.0 g samples of air dried soil (mass measured with precision to 0.1 mg). The SE scheme resulted in six chemically-distinct REY fractions associated with the following operationally-defined solid phase pools (see Table 2): adsorbed (exchangeable) species (Step 1), reducible Mn-oxides (Step 2), organo-metal complexes and dispersible colloids (Step 3), reducible short range order (SRO) Fe-oxides (Step 4), long range order (LRO) Fe-oxides (Step 5), and residual solids (silicates or primary mineral phosphates). Each extraction step was followed by a rinse with ultrapure water for 30 min with a 1:20 solid to solution mass ratio at room temperature. Extractions and rinses were shaken at 100 rpm followed by centrifugation at 44,000 relative centrifugal force (RCF) for 30 min and finally filtered through a 0.2 μm cellulose acetate membrane. The rinses were combined with the supernatant solutions for each extraction, with the residual solids subjected to further extraction. Soil-free controls ('blanks') for the five steps were carried out in triplicate as well.

REY and major cation concentrations in pore water and extraction solutions were determined by ICP-MS equipped with a dynamic reaction cell (DRC) to eliminate mass interferences (Perkin Elmer DRC II, Shelton, CT). The aqueous certified reference materials (CRM) were NIST 1643e (trace metals) and similar "second source" standards from Inorganic Ventures (Christiansburg, VA) and High Purity Standards (Charleston, SC). Rhodium (Rh) was included as an internal standard for Fe, Al, Mn, and P and indium (In) was used for REY based on

Table 2
Sequential extraction scheme used in the soils at La Jara ZOB. Mass:volume ratio, shaking time, and extraction temperature are also included.
Adapted from Laveuf et al. (2012) and Land et al. (1999).

Step	Phases	Procedure
1	Adsorbed, exchangeable, and carbonate bound	1.0 M CH_3COONa with CH_3COOH 99–100% Adjust pH to 5.5 1:10 m/V 1 extraction, shake 6 h, room temperature
2	Mn-oxides, e.g. birnessite	0.1 M $NH_2OH\cdot HCl$ in 0.1 M HCl Adjust pH to 2 1:20 m/V 2 extractions, shake 0.5 h, room temperature
3	Organo-metal colloids	0.1 M $Na_4P_2O_7$ Adjust pH to 10 1:10 m/V Shake 1.5 h, room temperature
4	Short range order (SRO) Fe-oxides, e.g. ferrihydrite	0.25 M $NH_2OH\cdot HCl$ in 0.25 M HCl Adjust pH to 1.5 1:20 m/V 2 extractions, 2 h each, 60 °C
5	Long range order (LRO) Fe-oxides, e.g. goethite	1.0 M $NH_2OH\cdot HCl$ in 25% CH_3COOH 99–100% Adjust pH to 1 1:30 m/V 3 h, 90 °C

similarities in first ionization potential. Customized calibration standards were prepared for each sequential extraction step matching the matrix composition to that of the samples prepared for ICP-MS analysis to account for matrix interferences. The detection limits in ng L^{-1} for Y, La, Ce, Pr, Nd, Sm, Eu, Gd, Tb, Dy, Ho, Er, Tm, Yb, and Lu were 3.3, 0.1, 0.4, 0.02, 0.4, 0.7, 0.1, 0.6, 0.1, 0.1, 0.1, 0.1, 0.1, 3.7, and 10.2, respectively. DOC concentrations in pore water samples and those associated with the organo-metal colloids (Step 3) and SRO Fe-oxides (Step 4) were determined using a Shimadzu TOC-VCSH analyzer (Columbia, MD).

2.5. Mass balance and fractionation calculations

Plots of REY concentrations across the lanthanide series in geomedia are typically normalized to references to account for differences in natural abundance, thereby enabling assessment of their fractionation. References used in REY normalization include, but are not limited to, parent materials, soil horizons from the system under investigation or published means of standard references such as the upper continental crustal (UCC) or chondritic samples (Taylor and McLennan, 1981; Evensen et al., 1978; Anders and Grevesse, 1989). Given that the objective of this study was to elucidate fractionation of REY among various secondary phases in weathering soil, REY concentrations per unit mass of sample for each extraction (ng kg^{-1}) were normalized by the total corresponding elemental mass concentration for the genetic horizon for which the extraction was performed. REY patterns are normally presented with a logarithmic y-axis, however, in the present study, small REY patterns variations were observed, therefore a linear scale was chosen. Non-dimensionalized cerium and europium anomalies (Ce/Ce*, Eu/Eu*) were calculated as (Braun et al., 1998):

$$\frac{Ce}{Ce^*} = \frac{Ce}{(La)^{0.5} \times (Pr)^{0.5}} \quad (1)$$

$$\frac{Eu}{Eu^*} = \frac{Eu}{(Sm)^{0.5} \times (Gd)^{0.5}} \quad (2)$$

where Ce, La, Pr, Eu, Sm, and Gd correspond to REE mass per unit mass of soil released in a given extract normalized by the total corresponding mass concentration for a given genetic horizon. Ce/Ce* or Eu/Eu* values higher than unity represent positive anomalies (enrichment), whereas values lower than unity represent negative anomalies (depletion) relative to the reference.

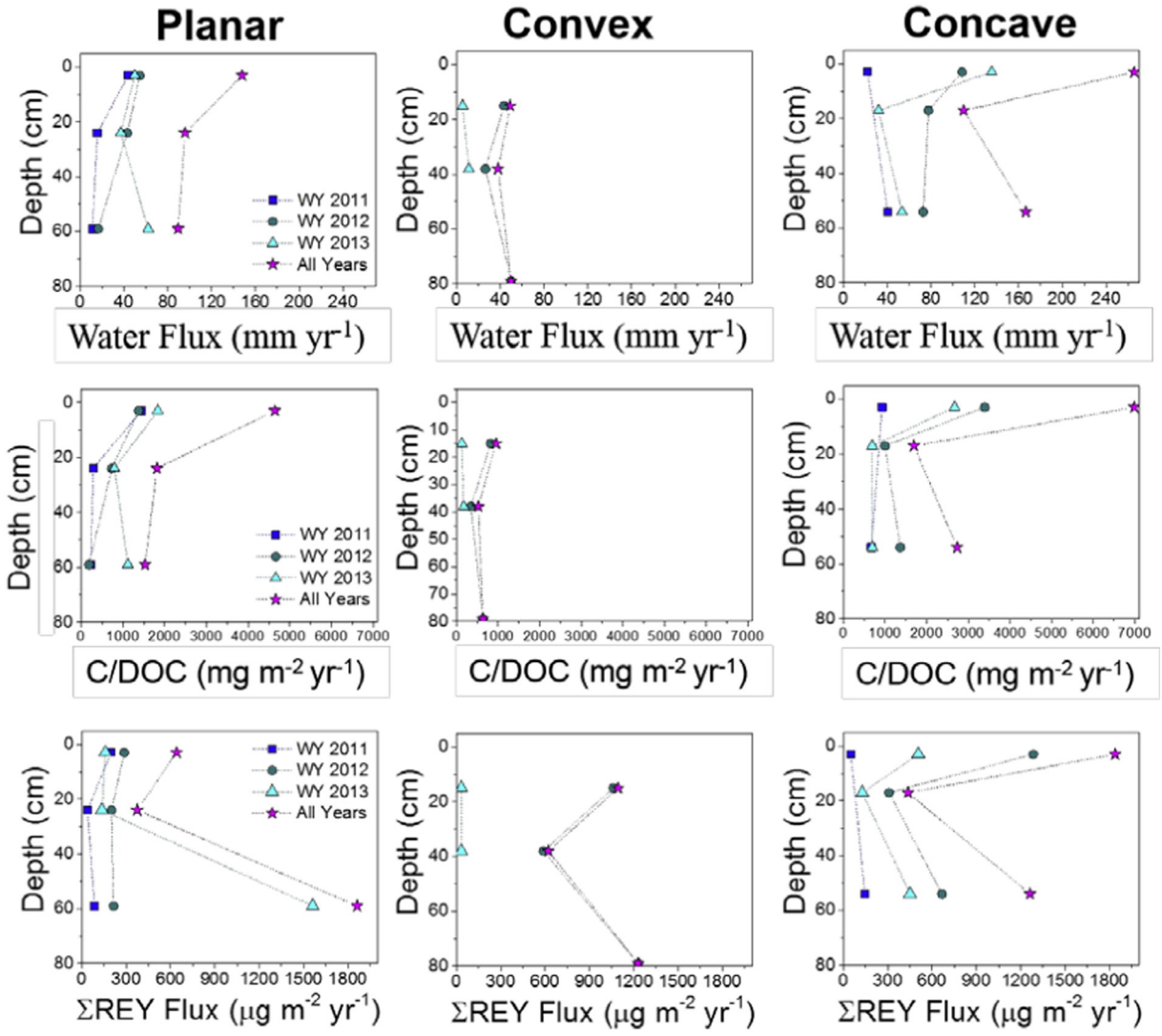

Fig. 2. Water (*top*), dissolved organic carbon (*middle*), and ∑REY (*bottom*) fluxes through depth increments of the planar (*left*), convex (*center*) and the concave (*right*) hillslope profiles. Total fluxes are shown for water years 2011, 2012, and 2013.

Chemical enrichment or depletion (tau) values relative to parent rock for bulk soils collected at the ZOB were determined as (Chadwick et al., 1990):

$$\tau_{Ti,j} = \frac{C_{a,soil}}{C_{a,parent}} \times \frac{C_{Ti,parent}}{C_{Ti,soil}} - 1 \quad (3)$$

where Ti was employed as an "immobile" element, C_a and C_{Ti} correspond to the REY or Ti concentrations in bulk soil or parent materials (mg kg^{-1}), and C_{Ti} corresponds to Ti concentration in the parent material (mg kg^{-1}). To permit direct comparison of the REY tau values for all hillslope profiles, REY concentration data were normalized to a weighted average of ZOB bedrock concentrations. Because both porphyritic rhyodacite and altered Bandelier Tuff contribute to parent rock composition of the site, their fresh rock compositions were analyzed for REY concentrations, and the mean REY signatures were calculated from the mapped fractional coverage of the two bedrock types in the ZOB (http://geoinfo.nmt.edu/publications/maps/geologic/ofgm/). The weighted average bedrock values were based on the fractional abundance of the porphyritic rhyodacite (0.44) and zeolitilized Bandelier Tuff (0.56) in the ZOB (Vázquez-Ortega et al., 2015). Tau values higher than (less than) zero represent enrichment (depletion) relative to parent rock.

3. Results

3.1. Fluxes of water, DOC and REY in planar, convex and concave Pedon locations

The landscape location for Pedon 1 showed intermediate values for topographic wetness index (TWI), as well as water and DOC fluxes (Table A.1, Appendix). Plan, profile and combined values were very close to zero giving this location a planar curvature characterization. Conversely, Pedon 3 exhibited convex curvature, whereas Pedon 5 displayed a concave curvature, based on plan curvature characterization and field observations. Pedon 5 also consistently showed the highest TWI, water and DOC fluxes among all profiles.

The planar, convex and concave hillslope locations exhibited distinct patterns in water, DOC, and REY through-flux (Fig. 2). The concave site showed higher pedon through-fluxes of water (109 to 265 mm y^{-1}), DOC (1700 to 7000 mg m^{-2} y^{-1}), and REY (440 to 1840 μg m^{-2} y^{-1}) (Fig. 2), as well as a greater accumulation of solid phase OC at depth (Fig. A.1, Appendix).

3.2. REY fractionation as a function of landscape location and soil depth

The planar, convex and concave hillslope locations exhibited different REY chemical depletion/enrichment patterns (tau plots) (Eq. (3)

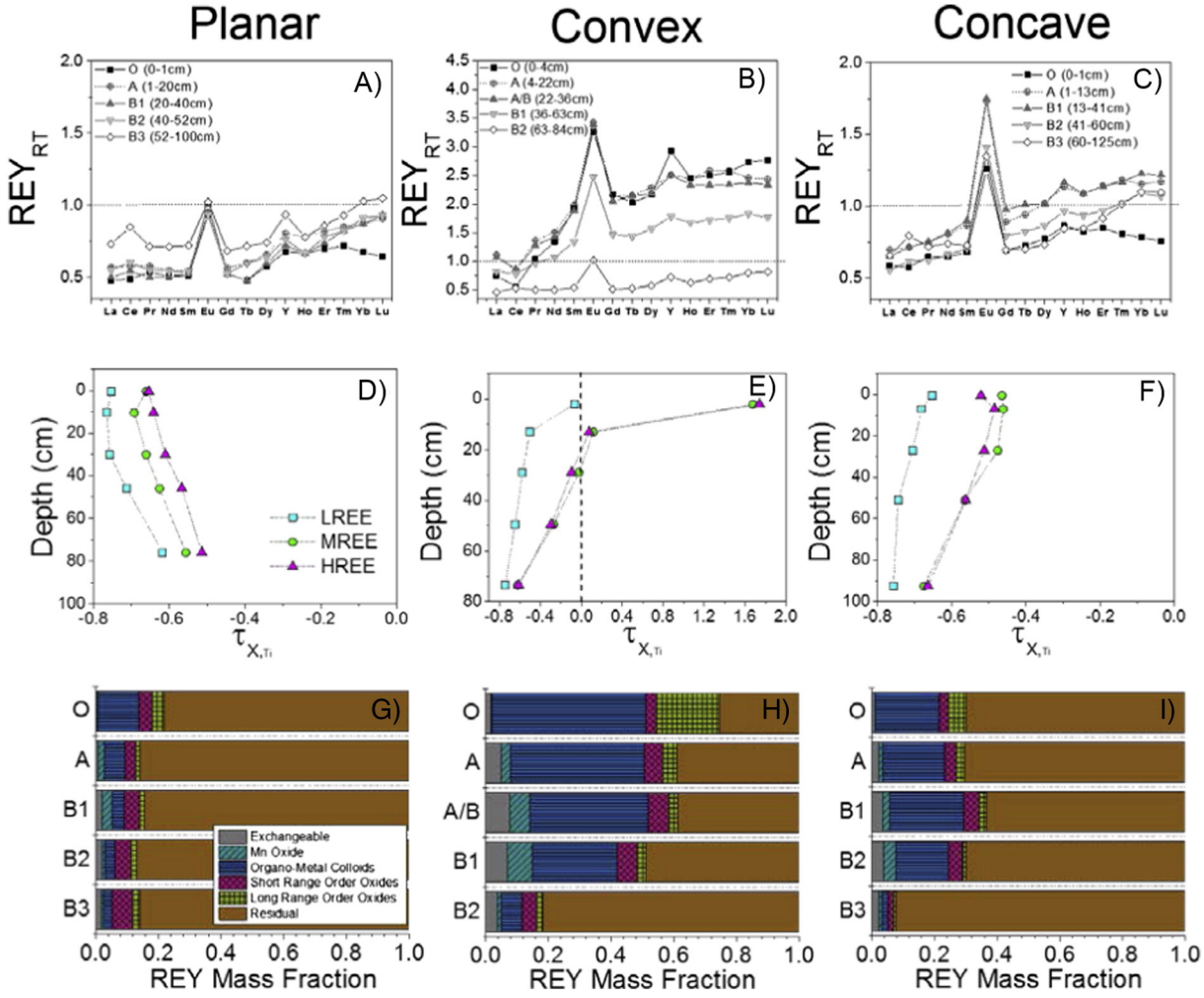

Fig. 3. REY fractionation patterns for the total solid phase (*top*), REY chemical depletion/enrichment patterns (i.e., tau plots, *middle*) and extractability patterns (*bottom*) as a function of depth in planar (*left*), convex (*center*) and concave (*right*) hillslope profiles. REY values for top row figures were normalized to the ZOB weighted average (RT) bedrock composition, whereas the middle row figures were based on bedrock (RT) normalized REE/Ti concentration ratios. Mass fractions are labeled with the names of the target phases, and are associated with the following chemical extractions: 1.0 M CH_3COONa (pH 5.5), 0.1 M $NH_2OH{\cdot}HCl$ (pH 2), 0.1 M $Na_4P_2O_7$ (pH 10), 0.25 M $NH_2OH{\cdot}HCl$ (pH 1.5), and 1.0 M $NH_2O{\cdot}HCl$ (pH 1). LREE, MREE, and HREE represent light, medium, and heavy rare earth elements, respectively. LREE = La to Nd, MREE = Sm to Tb, HREE = Dy to Lu (Y not included).

(p-values < 0.05) in the solid phase for the light, medium and heavy REY (LREE, MREE and HREE) (Fig. 3D, E and F). Light REE consistently showed greater depletion than MREE or HREE in all profiles. The upper horizons in the concave site were more depleted in REY when compared to the planar site and these horizons were also subjected to higher water and DOC fluxes (Figs. 3D, E and F). One noteworthy result is that the patterns of the convex location are very different from those of the planar and concave slopes.

Solid phase REY totals were differentially fractionated across operationally-defined solid phase pools as shown for the three pedon locations (Fig. 3G, H, and I). In the planar profile, the largest REY fraction was associated with the residual pool, ranging from 0.78 to 0.87, depending on depth (Fig. 3G). Among all pools targeted in the SE (with the exception of the residual pool), "organo-metal colloids" comprised the largest fraction of the O horizon, and in the planar profile, this pool showed a decreased relative prevalence with depth (from 0.13 to 0.03). The second most abundant fraction was released during extraction of SRO Fe-oxides, and this fraction showed an increased relative abundance with depth (from 0.03 to 0.07). A small "exchangeable" REY fraction increased with depth (from 0.004 to 0.02) as well, whereas the fraction of Mn-oxide associated REY was highest in the B1 horizon (0.03). A small (0.01 to 0.04) fraction was consistently released during extraction targeting LRO Fe-oxides.

In the concave site, REY abundance in extracted fractions decreased in the order: residual (0.63 to 0.92), organo-metal colloids (0.02 to 0.23), SRO Fe-oxides (0.02 to 0.05), LRO oxides (0.009 to 0.05), exchangeable (0.01 to 0.04), and Mn-oxides (0.002 to 0.04). For the convex site, REY abundance in extracted fractions decreased in the order: residual (0.25 to 0.83), organo-metal colloids (0.07 to 0.50), LRO oxides (0.02 to 0.2), SRO Fe-oxides (0.03 to 0.07), exchangeable (0.02 to 0.05), and Mn-oxides (0.003 to 0.08). Organo-metal colloids comprised a much larger fraction of the total REY pool in the convex and concave (relative to planar) hillslope profiles, particularly at depth.

3.3. REY signatures of extractable pools

To explore radius-dependent fractionation trends, REY patterns were plotted for all SE extraction steps using the convention of Bau and co-workers (Bau et al., 1995; Bau, 1999; Thompson et al., 2013), where Y is included to the left of Ho, consistent with its ionic radius (Figs. 4–5). These plots (discussed in order of SE steps, below) revealed that lanthanide contraction with increasing Z affects fractionation of REY among operationally-defined pools for all soil samples (Figs. 4–5). Extractable mean REY and major cation concentrations as a function of depth for the planar, convex and concave hillslope profiles are presented in Tables A.2–A.7 (Appendix). Also, mass fraction patterns for major cations and REY are presented in Figs. A.2–A.5 (Appendix).

3.3.1. Exchangeable REY

Step 1 targeted REYs adsorbed to negatively-charged soil particle surfaces and that were exchangeable with Na^+ at pH 5.5. In all locations, the exchanged REY showed an enrichment in MREE relative to HREE (planar: ΣMREE/ΣHREE ranging from 1.7 to 3.9; concave: ΣMREE/ΣHREE ranging from 1.1 to 1.7) (Fig. 4A, D and G). Exchangeable REY

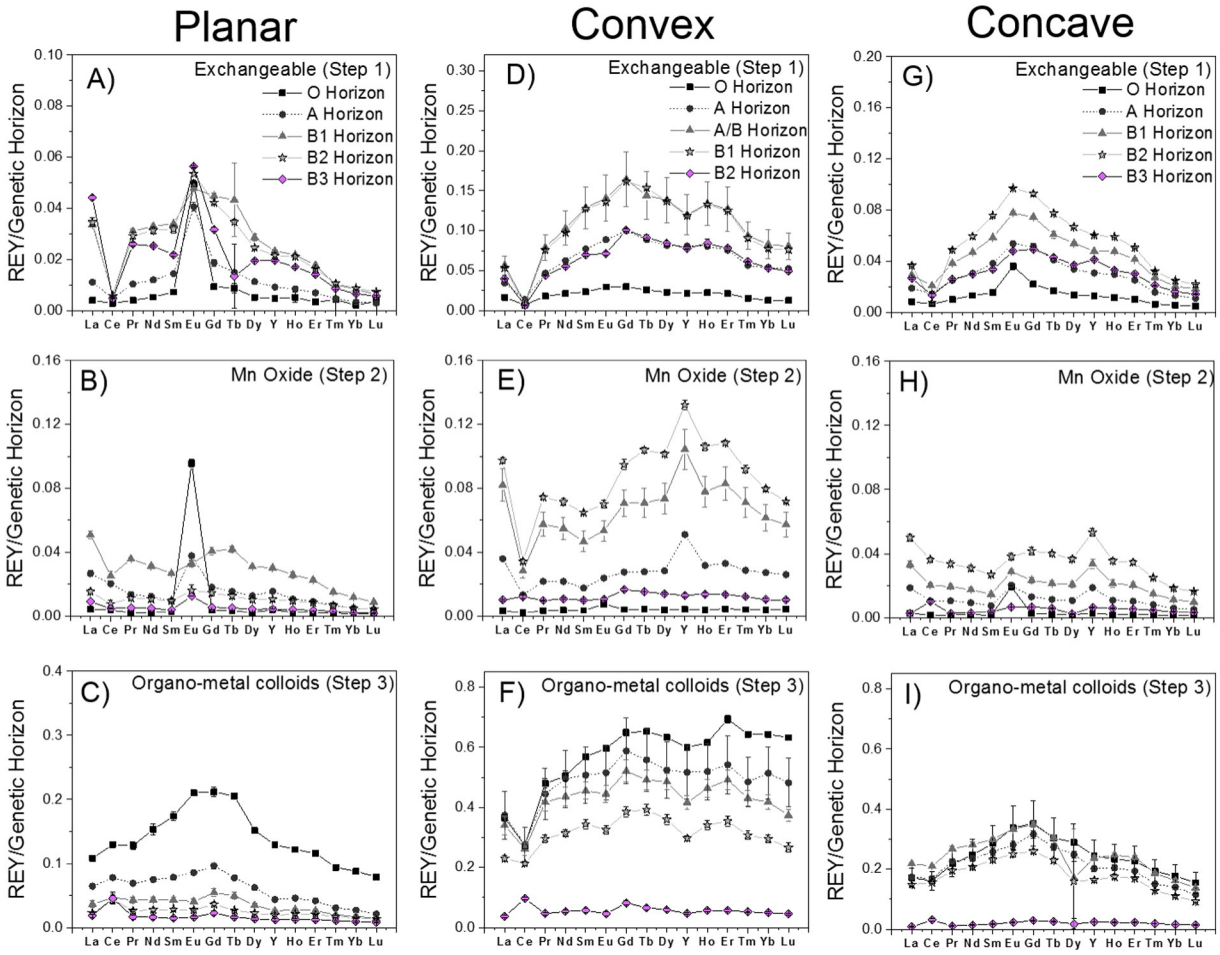

Fig. 4. REY fractionation patterns for the total REY fraction released during the sequential extraction in the planar (*left*), convex (*center*), and concave (*right*) hillslope profiles for the following operationally defined pools: exchangeable, Mn-oxide (i.e., birnessite), and organo-metal colloids. Error bars (standard deviations) were calculated from triplicate samples.

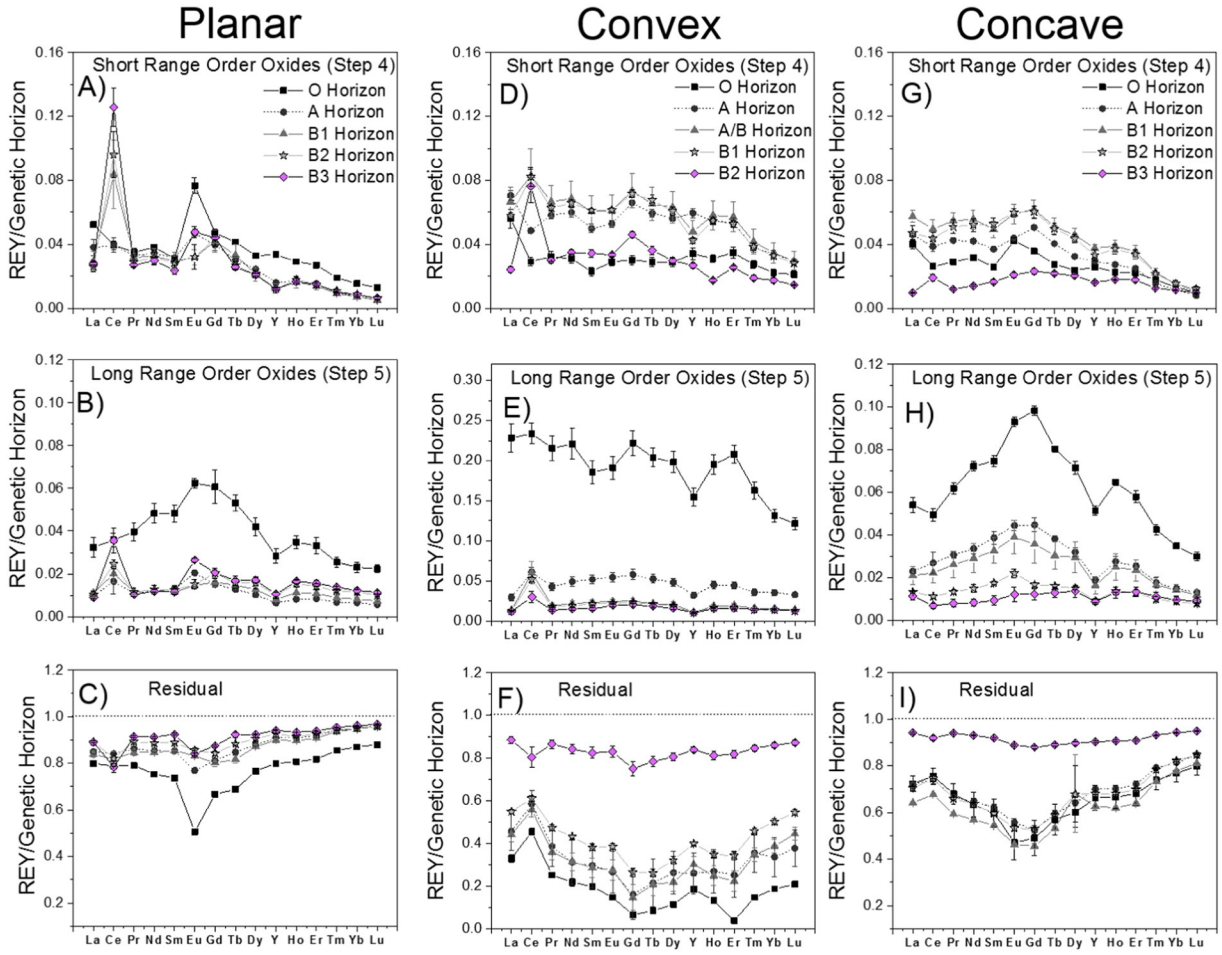

Fig. 5. REY fractionation patterns for the total REY fraction released during the sequential extraction in the planar (*left*), convex (*center*), and concave (*right*) hillslope profiles for the following operationally defined pools: short range order Fe-oxides (i.e., ferrihydrite), and long range order Fe-oxides (i.e., goethite), and residual. Error bars (standard deviations) were calculated from triplicate samples.

also exhibited negative Ce-anomalies (Ce/Ce^*) ranging from 0.14 to 0.72, from 0.11 to 0.42, and from 0.18 to 0.71 for the planar, convex and concave sites, respectively (Figs. 4A, D and G and 6A). A pronounced positive Eu-anomaly was observed for this extraction in the upper horizon of the planar site (Eu/Eu^* value equal to 6.0) (Fig. 7A). No systematic variations in Y/Ho ratios were observed in the "exchangeable" REY fraction (Fig. 8A).

3.3.2. Mn-oxide-bound REY

Only the deepest subsurface (B3) horizon in the concave profile showed a pronounced positive Ce anomaly ($Ce/Ce^* = 3.8$) in the Mn-oxide extractable fraction (Fig. 6B). In the convergent and planar soil profiles, the Mn-oxide extraction gave rise to a pronounced positive Eu-anomaly (Eu/Eu^*) in the upper horizon (planar: $Eu/Eu^* = 31$; convergent: $Eu/Eu^* = 10$) (Fig. 7B). This fraction exhibited Y enrichment with an apparent decrease in Y/Ho ratio with depth (planar: decreasing from 1.7 to 1.1; convex: decreasing from 1.6 to 0.94; concave: decreasing from 1.7 to 1.1) (Fig. 8B), but this trend was statistically significant (p-value < 0.05) only for the concave site.

3.3.3. REY in organo-metal colloids

In surface horizons of the planar site, Na-pyrophosphate dispersible organo-metal colloids showed MREE enrichments ($\Sigma MREE/\Sigma HREE$) ranging from 1.23 to 1.48 (Fig. 4C). In contrast, the deepest horizon exhibited a slight LREE enrichment, largely attributable to a positive Ce anomaly (B3 horizon: $\Sigma LREE/\Sigma HREE = 1.4$). The organo-metal colloid pool exhibited a depth-dependent increase in Ce/Ce^* (ranging from 1.1 to 2.6) (p-value < 0.05) (Fig. 6C). In the concave site pedon, organo-metal colloids in all horizons showed a MREE enrichment ($\Sigma MREE/\Sigma LREE$ ranging from 1.3 to 1.6) (Fig. 4F). Only the lower horizon exhibited a pronounced Ce-anomaly (convex: $[Ce/Ce^*] = 2.3$; concave: $[Ce/Ce^*] = 3.1$) (Fig. 6C) in the convex and concave sites. No systematic variations in Eu-anomalies were observed in organo-metal colloids (Eu/Eu^* ranges from 0.83 to 0.89) (Fig. 7C). In general all sites were depleted in Y (as determined from Y/Ho ratios) (Fig. 8C). Colloidal organic carbon (OC) in the planar and convex hillslope soils decreased as a function of depth, but in the concave soils it remained relatively high and similar that measured in the upper horizons (Fig. 9A and B).

3.3.4. SRO Fe-oxide-bound REY

Extracts targeting SRO Fe-oxides were depleted in HREE ($\Sigma LREE/\Sigma HREE$ ranged from 1.2 to 2.7 and 0.6 to 1.4 for planar and concave sites, respectively) (Fig. 5). This extraction revealed an increase in Ce/Ce^* as a function of depth for the planar site (from 0.9 to 4.6, regression p-value < 0.05), whereas for the convex and concave profiles, only the bottom horizons exhibited a positive Ce-anomaly (convex: $[Ce/Ce^*] = 2.8$; concave: $[Ce/Ce^*] = 1.8$) (Fig. 6D). Slightly positive Eu-anomalies were observed for upper horizons in all sites (Fig. 7D). The SRO Fe-oxide fraction showed preferential uptake of Ho (relative to Y) in bottom horizons in all profiles (Fig. 8D). Lower OC concentrations were observed in the SRO Fe-oxide extraction as compared to the organo-metal colloid extraction (Fig. 9).

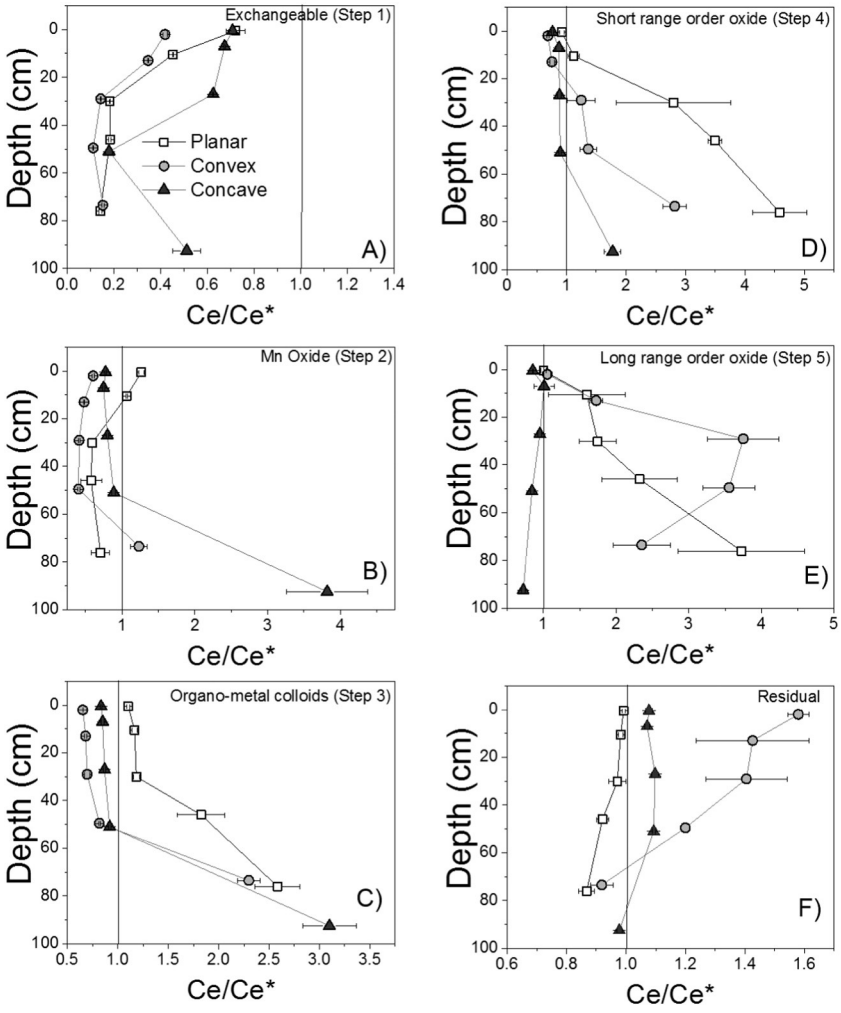

Fig. 6. Ce/Ce* values normalized to the each genetic horizon in the planar, convex and concave hillslope profiles for the following fractions: (A) exchangeable, (B) Mn-oxide (i.e., birnessite), (C) organo-metal colloids, (D) short range order Fe-oxides (i.e., ferrihydrite), (E) long range order Fe-oxides (i.e., goethite), and (F) residual. The Ce/Ce* values were calculated from the Ce fraction released during the sequential extraction. Error bars were calculated from triplicate samples. Ce/Ce* higher than 1 represent positive anomalies (Ce enrichment) and values lower than 1 represent negative anomalies (Ce depletion).

3.3.5. LRO Fe-oxide-bound REY

In the planar profile, a small fraction of REY was associated with the LRO Fe-oxides, dominantly represented by goethite in these soils (Vázquez-Ortega et al., 2015) (Fig. 3G). An increase in Ce/Ce* was observed as a function of depth in the planar site for LRO Fe-oxides (Fig. 6E), similar to the trend observed for SRO Fe-oxides. In contrast, Ce/Ce* values in the concave site soils did not exhibit systematic variation (Fig. 6E). The convex site also exhibited positive Ce-anomalies. The Eu/Eu* values for these extracts ranged from 0.96 to 1.73 (Fig. 7E). The data indicated preferential uptake of Ho (relative to Y) into LRO Fe-oxides in all sites (Fig. 8E). Linear regression analysis indicated that depth-dependent trends in Y/Ho ratio were statistically significant (p-value < 0.05) only for the planar site.

3.3.6. Residual REY signatures

Residual (non-extracted) materials in all profiles showed a concave upward pattern, and this was particularly evident for the concave site, signaling residual retention of LREE and HREE, with preferential transfer to extractable weathering products of MREE (Fig. 5C, F and I). Ce/Ce* values of SE residual decreased with depth in the planar and convex hillslope sites (p-value < 0.05) (Fig. 6F). No systematic variation in Eu amnomalies was observed in the residual materials for the planar and convergent profiles, but slighty positive anomalies were observed in the convex (Fig. 7F). Also, no systematic variations in Y/Ho ratios were observed in the residual fraction for the planar and concave profiles (Fig. 8F), whereas in the convex site it exhibited a small Y enrichment.

4. Discussion

Prior published work indicates that multiple competing processes (aqueous complexation, solid-solution particitioning, biouptake) affect REY fractionation over the course of biogeochemical weathering of the critical zone (Weill and Drake, 1973; Sholkovitz, 1992; Braun et al., 1993; De Carlo and Wen, 1998; Panahi et al., 2000; Ohta and Kawabe, 2001; Pokrovsky and Schott, 2002; Davranche et al., 2004; Johannesson et al., 2004; Davranche et al., 2005; Steinmann and Stille, 2006; Pourret et al., 2007a; Steinmann and Stille, 2008; Laveuf and Cornu, 2009; Pourret et al., 2010; Davranche et al., 2011; Xiong, 2011; Vázquez-Ortega et al., 2014). The current work builds on these prior studies to show that while chemical denudation of REY depends on co-mobilization with complexing ligands, a variety of solid-phase weathering products (quantified here on the basis of sequential chemical extraction) remain in the regolith residuum comprising distinct pool-specific signatures. Further, our data suggest that hydrologic flow patterns associated with different landscape locations (Fig. 2) alter the relative importance of different solid phase REY pools and their depth-dependent retention in soil (Fig. 3).

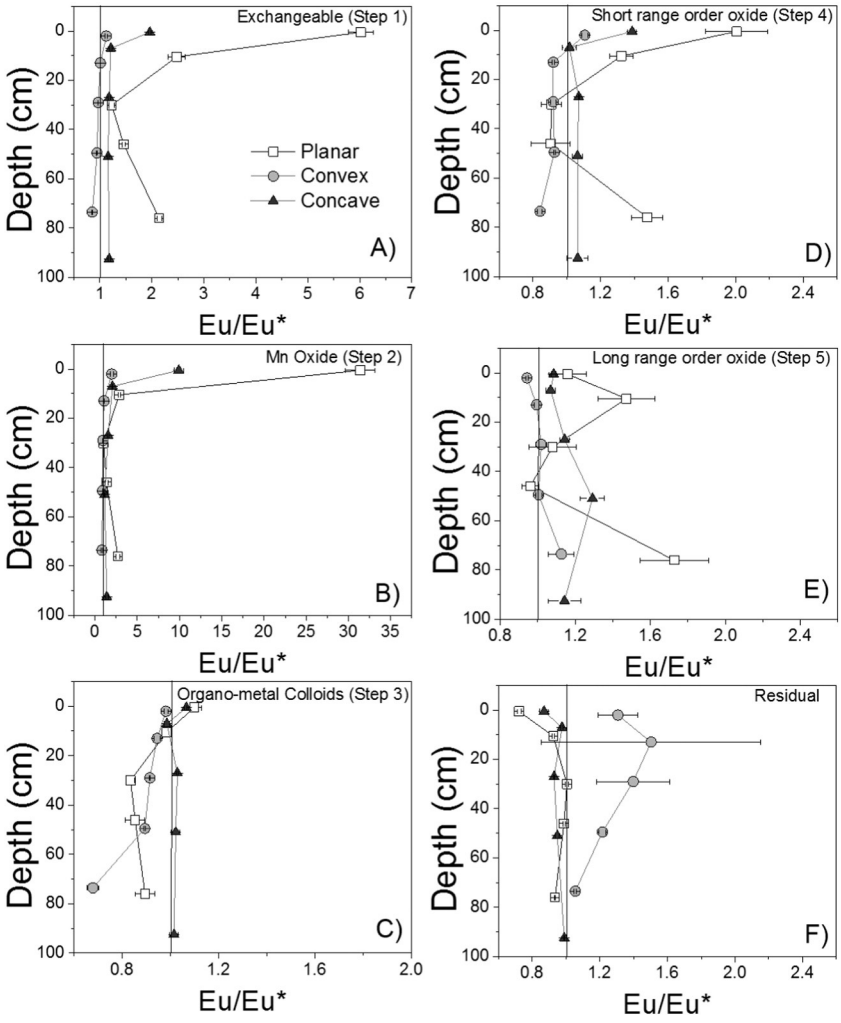

Fig. 7. Eu/Eu* values normalized to the each genetic horizon in the planar, convex and concave hillslope profiles for the following fractions: (A) exchangeable, (B) Mn-oxide (i.e., birnessite), (C) organo-metal colloids, (D) short range order Fe-oxides (i.e., ferrihydrite), (E) long range order Fe-oxides (i.e., goethite), and (F) residual. The Eu/Eu* values were calculated from the Eu fraction released during the sequential extraction. Error bars were calculated from triplicate samples.

The coherency of lanthanide series geochemical fractionation patterns as a function of soil depth (e.g., Figs. 4 and 5) can be traced to variation in chemical parameters controlling REY geochemical reactivity: ionic potential, Lewis acidity, Misono softness, and the associated polyvalent cation partitioning at the interface between mobile pore fluids and secondary organo-mineral weathering products (Laveuf and Cornu, 2009; Pourret et al., 2010; Thompson et al., 2013). Regolith REY patterns depend on how radius or electronic structural differences influence REY reactivity toward (1) stable complexation with inorganic and organic ligands, (2) surface complexation and co-precipitation with solid-phase weathering products, and (3) oxidation–reduction reactions. The current study demonstrated that the net result of competition among these reactions in soils is preferential light REE depletion (depth-dependent chemical depletion or enrichment trends as depicted in tau plots) (Fig. 3D, E, and F).

Trends in porous media depletion of REE (Fig. 3D, E, and F) are consistent with those of water and carbon through-flux (Fig. 2). However, these trends are insufficient to resolve the biogeochemical mechanisms controlling REY patterns retained in the weathered regolith; the total regolith REY pattern (Fig. 3A, B, and C) is the linear combination of distinct secondary phase products. Hence, we determined the mass balance of REY partitioned into selectively-extracted, solid-phase pools as a means to assess the relative importance of various weathering products in REY stabilization. One noteworthy result is that across all samples, and irrespective of landscape position, soils subjected to a given chemical extraction exhibited similar REY patterns (Figs. 4 and 5), even though their relative contributions to the total mass of solid phase REY were highly variable within and between pedons (Fig. 3G, H, and I). This indicates consistent affinity trends across the REY for partitioning into sequentially-extracted secondary solid phase pools during regolith development. Such trends include, e.g., enrichment of medium to heavy REE in exchangeable and organo-metal colloidal pools and a trend toward retention of HREE in residual material (Figs. 4 and 5). Another notable observation is that the streamwater REY patterns presented in Vázquez-Ortega et al. (2015) more strongly resemble the total soil solid phase (bulk) patterns than any of the extractable or residual fractions, including the solid-phase soil organic matter (SOM) colloid fraction.

To examine the impacts of soil biogeochemical properties on REY patterns, we correlated REY pattern parameters (e.g., MREE/REE, Ce*/Ce, Y/Ho) against soil chemical properties (organic carbon, mass of Fe and Mn oxide forms extracted, etc.). In doing so, we sought to assess the extent to which quantitative variations in these parameters were related to pedogenic composition of the soil samples across the entire set. As mentioned above, extract REY data were typically normalized against the totals for the genetic horizon for which the extraction was performed. However, to enable direct correlation against soil chemical parameters across all samples irrespective of pedon location,

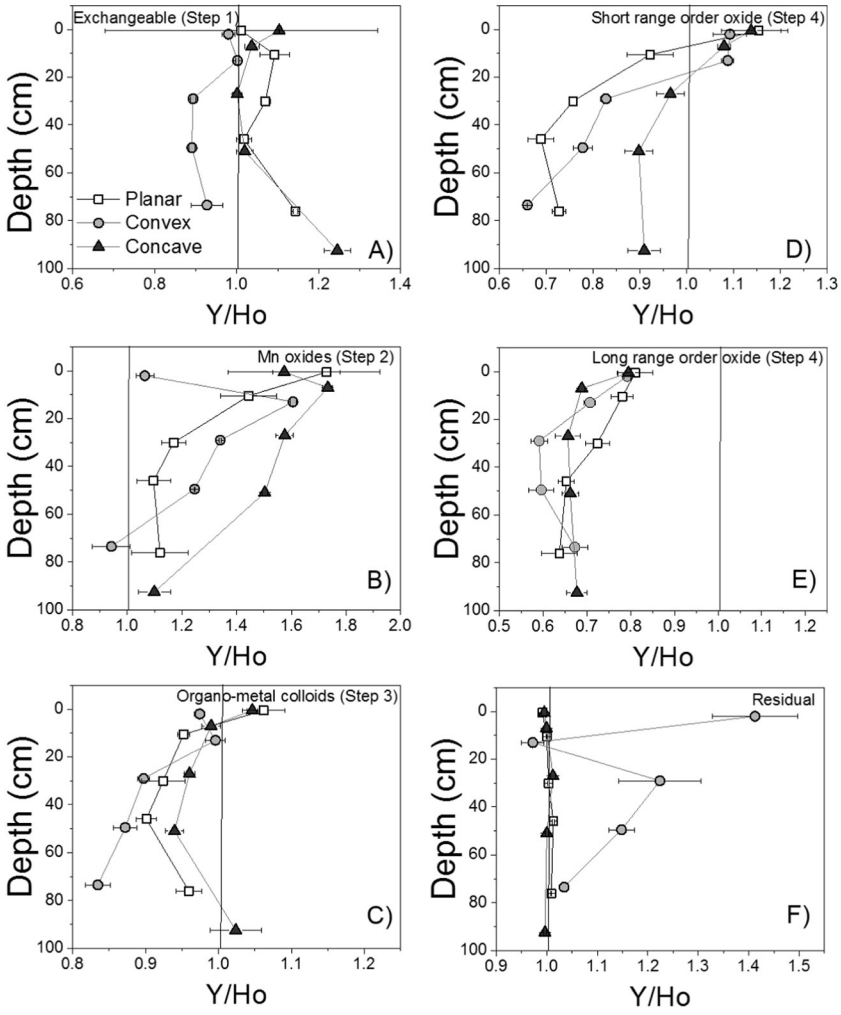

Fig. 8. Y/Ho ratios normalized to the each genetic horizon in the planar, convex and concave hillslope profiles for the following fractions: (A) exchangeable, (B) Mn-oxide (i.e., birnessite), (C) organo-metal colloids, (D) short range order Fe-oxides (i.e., ferrihydrite), (E) long range order Fe-oxides (i.e., goethite), and (F) residual. The Y/Ho ratios were calculated from the Y and Ho fractions released during the sequential extraction. Error bars were calculated from triplicate samples. Y/Ho ratios higher than 1 represent positive Y enrichment whereas values lower than 1 represent Y depletion.

statistical tests were also performed for REY extract data normalized (for all samples) against the weighted mean bedrock REY composition of the ZOB (Bedrock RT).

4.1. Role of water and dissolved organic carbon flux on REY fraction

The different patterns of water and DOC flux that occur in pedons located in planar, convex and concave hillslope positions (Fig. 2) – specifically variation in the contribution of subsurface lateral throughflow – was found to influence patterns of REY chemical depletion in regolith. For example, the planar site exhibited decreasing REY depletion with depth, a trend consistent with surface horizons that were subjected to significantly higher water flux (Figs. 2–3). The concave site showed higher DOC and water fluxes at depth (relative to the planar and convex) across all sampling dates over water years 2011, 2012, and 2013, as well as greater REY efflux (determined from $\sum$REY fluxes) relative to the planar site (with the exception of WY 2013) (Fig. 2), a hydrochemical pattern that was consistent with greater solid phase depletions of REY at depth (Fig. 3). Taken together, these aqueous and solid phase geochemical results are consistent with organic ligand-promoted REY fractionation between mobile fluids and weathering residuum.

The convex site is located on a steep slope receiving colluvial inputs (Table A.1, Appendix) wherein poor drainage has also given rise to redoximorphic features (data not shown). The upper horizons in the convex site displayed the largest enrichment in the LREE, MREE, and HREE fractions among all study sites. A plausible explanation for this enrichment is colluvial delivery of REY-organic complexes, because this is consistent also with the large mass fraction of REY associated with the organo-metal colloidal fraction (Fig. 3). The REY mass fractions associated with the organo-metal colloid pool (whether normalized to the genetic horizon or to bedrock) were positively correlated with the corresponding OC concentrations extracted also from this pool (genetic horizon: $R^2 = 0.68$, p-value > 0.05; bedrock: $R^2 = 0.73$, p-value > 0.05) (Table 3 and Fig. 10A and C). The same extraction scheme also revealed a large uranium (U) enrichment in the upper horizons of the convex site that was also attributed to an association of U with the organo-metal colloid pool (Huckle et al., submitted for publication). Also as noted previously, dust inputs may contribute significantly to soil REY measurements, particularly in near surface horizons (Vázquez-Ortega et al., 2015).

4.2. REY signature of soil organic matter

Among all pools targeted in the SE (with the exception of the residual pool), dispersible organo-metal colloids contained the largest mass fraction of REY (Fig. 3G, H, and I). REY concentrations associated with the organo-metal colloid fraction in the convex and concave sites remained relatively high and similar across the top four horizons of

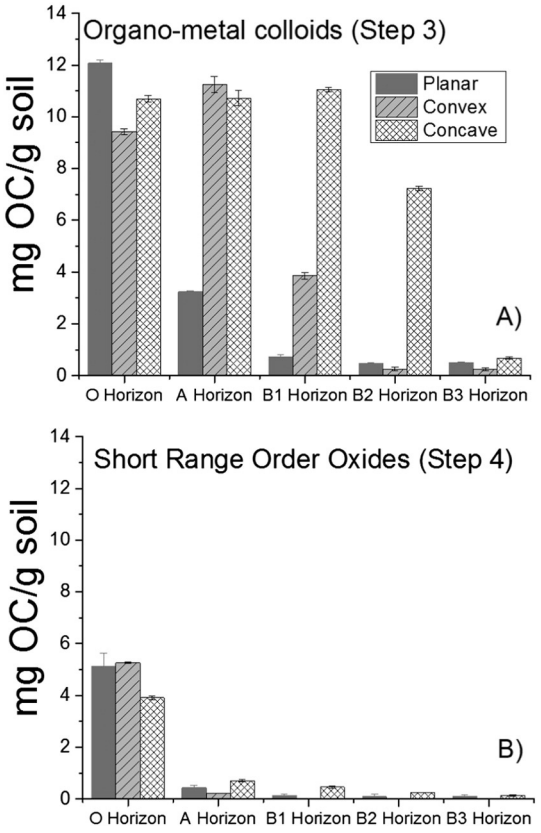

Fig. 9. Organic carbon associated released during the (A) organo-metal colloid and (B) SRO Fe-oxide steps of the sequential chemical extraction for all genetic horizons in the planar, convex and concave hillslope profiles.

the soil profile. As trivalent metals, REY form stable organo-metal complexes with OM (Byrne and Li, 1995; Sonke and Salters, 2006; Goyne et al., 2010; Yamamoto et al., 2005, 2010). Complexes with OM usually favor REE of intermediate (MREE, from Sm to Tb) and heavy (HREE, from Dy to Lu) mass that, because of their smaller ionic radii, tend to form more stable complexes with carboxyl and phenolic hydroxyl groups (Schijf and Byrne, 2001; Sonke and Salters, 2006; Pourret et al., 2007b; Pourret and Martinez, 2009; Tang and Johannesson, 2010a).

The MREE enrichment evidenced in the REY patterns of the dispersible colloidal fraction, indicating preferential MREE transfers from primary phosphates or silicates to secondary organic and Al-, Fe-(oxy)hydroxide colloids phases (Fig. 4C, F, and I), is consistent with MREE enrichment of these organic-rich secondary solids. In the planar location, a positive correlation between MREE/LREE ratios (normalized to genetic horizon) and OC obtained from the organo-metal colloid pool ($R^2 = 0.76$, p-value < 0.05) was observed (Table 3 and Fig. 10). A linear regression analysis indicates a positive correlation between Ga/La ratios and OC obtained from the organo-metal colloid pool in the concave location ($R^2 = 0.81$, $p < 0.05$) (Table 3). Also, a positive correlation between MREE/LREE ratios and OC (organo-metal colloid pool) ($R^2 = 0.32$, p-value < 0.05) including all data normalized by the parent materials was observed (Table 3). Similarly, Tang and Johannesson (2010a) indicated that in the absence of organic ligands, a smaller mass of REE was extracted from aquifer sediments relative to when DOM-containing solutions were employed. They also observed an MREE downward concavity pattern in the DOM-enriched solutions, consistent with the MREE affinity for OM complexation, as indicated in the current work (Fig. 4C, F, and I). Likewise, MREE downward concavity patterns in soil solutions during wetland soil reduction have been reported, attributing to soil organic matter a tendency to concentrate MREE (Davranche et al., 2011). In addition, REE–DOM partition coefficient (K_d) patterns revealed that DOM can be enriched in MREE by means of competition of REE with Fe and Al for carboxylic binding sites (Marsac et al., 2012, 2013). Hence, we attribute the solid phase accumulation of MREE-enriched organic colloids to the aggregation of organic matter–REY complexes and their retention in regolith.

Molecular spectroscopy studies have shown that provenance of stream water DOM at the JRB-CZO site varies seasonally (Perdrial et al., 2014a). Lignin-derived polyphenols and carboxylates, characteristic of 'terrestrial' DOM, have dominated the early snowmelt to peak discharge period, whereas microbially-derived DOM, with protein and polysaccharide enrichment characteristic of greater reworking of plant-derived material, are most prevalent during the drier early summer and fall seasons (surrounding the north American monsoon July to September, during lower hydrologic discharge) (Perdrial et al., 2014a). In discovering that concave down REY patterns are associated with the solid-phase soil organic matter (SOM) pool (Fig. 4C, F, and I), the current study suggests that REY signatures may help to trace episodic mobilization of SOM and its transfer to surface waters. Indeed, our prior work has shown that highest surface water REY concentrations coincided with peak discharge that occurred during snowmelt (Vázquez-Ortega et al., 2015), and that this was accompanied by elevated DOC with a terrestrial spectroscopic signature (lignin-derived polyphenols and carboxylates) (Perdrial et al., 2014a). Because terrestrial SOM is observed to transfer to streams during the period of greatest catchment wetting (snowmelt period), we postulate that this SOM–REY correlation may be related to a shift in hillslope redox conditions. For example, reductive dissolution of Mn(IV) and Fe(III)-(oxy)hydroxides can release sorbed SOM into mobile porewaters (Thompson et al., 2006; Davranche et al., 2011), and these processes are most likely to ensue during short pulsed events, when soils are saturated during snowmelt.

4.3. Weathering controls on REY pattern formation

4.3.1. Processes that favor Ce anomalies in soil profiles

Cerium fractionation during mineral transformation is strongly influenced by oxidation–reduction reactions in soils (Braun et al., 1990; Davranche et al., 2011; Laveuf et al., 2012). The oxidation of Ce(III) under oxic conditions induces decoupling of Ce(IV) from the lanthanide group, promoting its solid phase incorporation, and generating positive Ce anomalies in oxic soils (Feng, 2010; Laveuf et al., 2012). Fe- and Mn-oxides have been reported to display positive Ce-anomalies because of Ce(IV) co-precipitation (De Carlo and Wen, 1998; Braun et al., 1990; Ohta and Kawabe, 2001; Laveuf et al., 2008; Laveuf et al., 2012; Bau, 1999; Bau and Koschinsky, 2009).

In the planar hillslope profile studied here, a large mass fraction of Ce was associated with the SRO Fe-oxide pool and Ce concentrations increased slightly with depth (Fig. A.2, Appendix). In contrast, in the convex and concave sites, Ce was mainly associated with the organo-metal colloid pool (Fig. A.2, Appendix). Distribution coefficients (K_d) for Ce reported by Ohta and Kawabe (2001) indicated that Mn-oxides have a higher affinity for Ce than for Fe-(oxy)hydroxides. However, our study shows an apparently higher Ce affinity for Fe-(oxy)hydroxides than for Mn-oxides (Fig. 6). Pronounced positive Ce-anomalies (planar and convex sites) were revealed after the reductive dissolution of the SRO and LRO Fe-oxides, and the magnitude of these anomalies increased systematically with depth (Fig. 6D and E). The SRO and LRO extractions exhibited a larger enrichment in Ce than did the total solid phase (data not shown). Mass balance values (tau values, in the total solid phase) for Ce were more similar to those of Fe than to Mn, also consistent with the association of Ce with Fe-oxides in the ZOB bulk soils (Fig. 11). It is noteworthy that Fe concentrations (reported in g kg^{-1}) in the bulk soils were several orders of magnitude higher than Mn concentrations (Table 1) and, hence, the higher abundance of Fe in the bulk soils could be responsible for more effective Ce sequestration into Fe-(oxy)hydroxides simply because of their greater abundance of reactive interfacial sites. In the planar location, positive correlations between

Table 3
Correlation coefficients between REY and soil chemical variables.

Location	REY variables	Soil chemical variables					
		OC (Organo colloids, S3)[a] (mg/g)	Fe (Bulk) (g/kg)	Fe/Mn ratio (bulk)	Fe (SRO, S4) (mg/kg)	Fe (LRO, S5) (mg/kg)	Mn (Mn oxide, S2) (mg/kg)
Individual pedons normalized by the genetic horizon							
Planar	REY mass fraction (organo colloids, S3)	0.98*					
	MREE/LREE (organo colloids, S3)	0.76*					
	Gd/La (organo colloids, S3)	0.68					
	Ce/Ce* (SRO, S4)		0.65	0.98*	0.33		
	Ce/Ce* (LRO, S5)		0.87*	0.92*		0.87*	
	Y/Ho (Mn oxides, S2)			0.73			0.91*
	Y/Ho (SRO, S4)			0.69			0.94*
	Y/Ho (LRO, S5)			0.92*			0.63
Convex	REY mass fraction (organo colloids, S3)	0.82					
	MREE/LREE (organo colloids, S3)	0.39					
	Gd/La (organo colloids, S3)	0.21					
	Ce/Ce* (SRO, S4)		0.30	0.66	0.20		
	Ce/Ce* (LRO, S5)		0.18	0.02		Negligible	
	Y/Ho (Mn oxides, S2)			0.12			0.40
	Y/Ho (SRO, S4)			0.23			Negligible
	Y/Ho (LRO, S5)			Negligible			0.37
Concave	REY mass fraction (organo colloids, S3)	0.96*					
	MREE/LREE (organo colloids, S3)	0.01					
	Gd/La (organo colloids, S3)	0.81*					
	Ce/Ce* (SRO, S4)		0.98*	0.93*	0.73		
	Ce/Ce* (LRO, S5)		0.50	0.55		Negligible	
	Y/Ho (Mn oxides, S2)			0.85*			0.50
	Y/Ho (SRO, S4)			0.55			0.67
	Y/Ho (LRO, S5)			0.24			0.46
All data set, including planar, convex and concave normalized by the parent materials							
	REY mass fraction (organo colloids, S3)	0.17					
	MREE/LREE (organo colloids, S3)	0.32*					
	Ce/Ce* (SRO, S4)			0.56*			
	Ce/Ce* (LRO, S5)			0.48*			
	Y/Ho (Mn oxides, S2)			0.37*			0.39*
	Y/Ho (SRO, S4)			0.37*			0.27*
	Y/Ho (LRO, S5)			0.01			0.01

S2, S3, S4, and S5 correspond to the sequential extraction Steps 2, 3, 4, and 5, respectively.
[a] Organic carbon associated with the organo-metal colloid pool.
* Correlation has p-value < 0.05.

Ce-anomalies obtained from the SRO and LRO pools normalized to the genetic horizons and Fe:Mn ratio (bulk soil) were observed (SRO: $R^2 = 0.98$, p-value < 0.05; LRO: $R^2 = 0.92$, p-value < 0.05) (Table 3 and Fig. 12). When the Ce-anomalies (SRO) in the concave location were normalized to the parent materials, a positive correlation between Ce-anomalies and Fe:Mn ratio (bulk soil) was revealed, indicating the greater affinity of Ce for the Fe-oxides (Table 3 and Fig. 12). Also, a positive correlation between Ce-anomalies (SRO and LRO) and Fe:Mn ratio (bulk soil) (SRO: $R^2 = 0.56$, p-value < 0.05; LRO: $R^2 = 0.48$, p-value < 0.05) including all data normalized by the parent materials was observed (Table 3). Similar to our results, Bau and Koschinsky (2009) observed positive Ce anomalies in Fe-oxides precipitated into marine ferromanganese crusts, suggesting that in marine systems, oxidative scavenging of Ce is not restricted to Mn(IV)-oxides, but also includes Fe(III)-oxides. The current results indicate that the same is true for soil systems.

Vázquez-Ortega et al. (2015) reported an incremental increase in positive Ce-anomalies (for samples normalized to parent rock) as a function of depth for the total solid phase of the same pedons. In addition, the study reported negative Ce-anomalies in soil solutions in the upper horizons of the planar site during snowmelt of WYs 2011 and 2012. The negative anomalies were consistent with the prevalence of oxic conditions favoring Ce(IV), which exhibits high solid phase retention relative to other REY (Feng, 2010). Conversely, soil solutions at the deepest depth sampled exhibited no anomalous behavior for much of the sampling period, and small negative Ce-anomalies during the later portion of the snowmelt period (WY 2011), indicating a progressive change in redox conditions from reducing to oxidizing, over the course of snowmelt at depth. As a result, Ce translocated from the surface during pulsed reducing events accumulated at depth in the soil profile upon reoxidation. Seasonal, depth-dependent redox effects, coupled with the systematic increase in positive Ce-anomalies in the bulk soil with depth (Vázquez-Ortega et al., 2015) and the results reported herein – showing significant positive Ce-anomalies in the SRO (i.e., ferrihydrite) and LRO (i.e., goethite) Fe-oxide pools – provide strong evidence for the role of redox-active Fe-oxides in Ce sequestration in the CZO soils.

4.3.2. Processes that favor Eu anomalies in soil profiles

Several physico-chemical processes have been implicated in the enrichment of Eu in products of geochemical weathering (soil, soil solution, stream water, and ocean), including dust deposition and preferential weathering of feldspar minerals (K-feldspar and plagioclases) (Douville et al., 1999; Ma et al., 2011; Brioschi et al., 2013; Vázquez-Ortega et al., 2015). Chadwick and co-workers (Chadwick et al., 1999; Kurtz et al., 2001; Porder et al., 2007) have documented the crucial role that dry atmospheric deposition (i.e., dust) plays in the replenishing lithogenic nutirents in Hawaiian soils, and this process also has implications for REY deposition/enrichment. Positive Eu-anomalies (for samples normalized to parent rock) were observed in the ZOB soil matrix (Fig. 3A, B and C), as well as in soil solutions, and stream waters in the JRB-CZO site (Vázquez-Ortega et al., 2015). Results from the present study provide some insight into biogeochemical processes during pedogenesis that influence the fractionation, transport, and fate of Eu in soils. Specifically, we observed positive Eu-anomalies in the upper horizons in the exchangeable, Mn-oxide, and SRO oxide

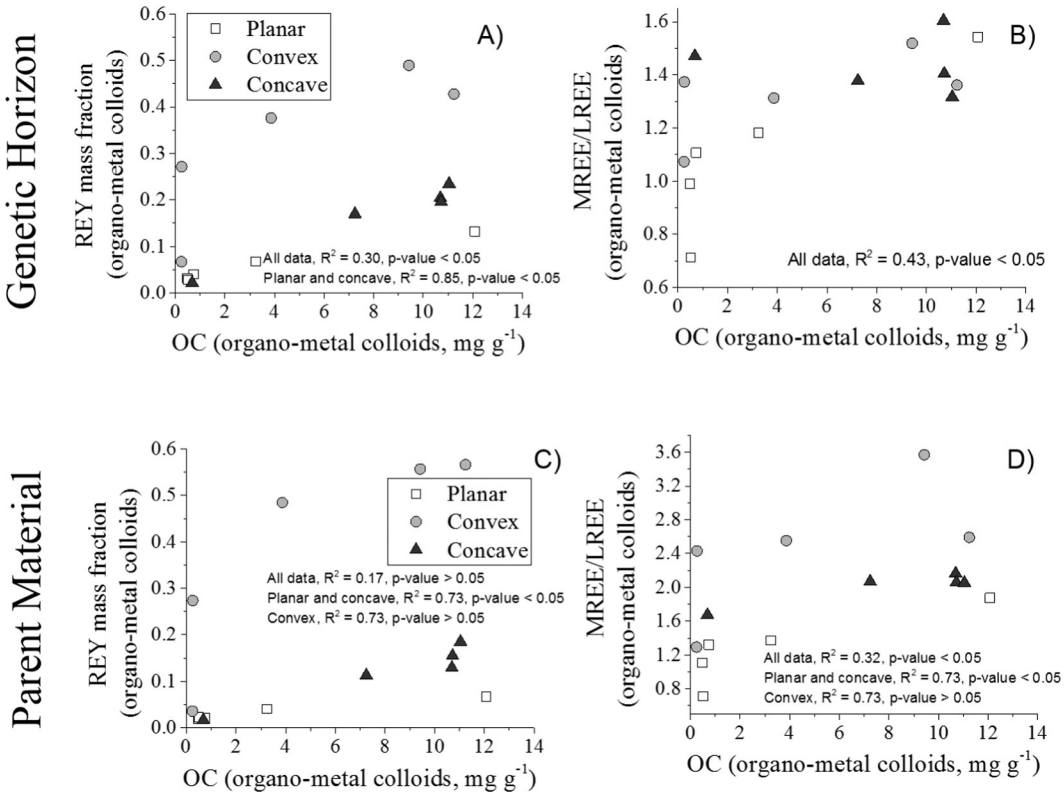

Fig. 10. Comparison between (A) REY mass fraction and (B) MREE/LREE normalized to the genetic horizon versus OC obtained from the organo-metal colloid pool. Also, comparison between (C) REY mass fraction and (D) MREE/LREE normalized to the parent materials versus OC obtained from the organo-metal colloid pool.

(only in the planar and concave sites) operationally-defined pools (Fig. 7). This was only observed in the uppermost 20 cm, indicating a strong influence of dust deposition on Eu enrichment and partitioning into secondary phases.

The mass fraction of Eu in the O horizon of the planar site profile (Fig. A.3, Appendix) clearly indicates a high mass of Eu associated with the Mn-oxide, SRO and LRO pools and an incremental decrease with depth. In the convex and convergent sites, organo-metal colloids are a primary repository for Eu (Fig. A.3, Appendix). (Oxy)hydroxide nano-particles and colloids, common weathering products in pedogenic environments, have been shown to be enriched in REY (Thompson et al., 2006) and their mobilization during redox fluctuations can facilitate their transport in soil and water systems (Guo et al., 2010b; Sholkovitz, 1992; Thompson et al., 2006). REY also exhibit variable metal–ligand stabilities with carboxyl and phenolic-OH functional groups of OM (Byrne and Li, 1995), which favors MREE (including Eu) enrichment (Davranche et al., 2011). Strong positive correlations between REE with DOC concentrations have been reported for stream waters at the JRB-CZO (Vázquez-Ortega et al., 2015), highlighting the fact that bio-ligands produced in the CZ mediated REE chemical denudation. In summary, consistent mineral dust inputs, adsorption/co-precipitation of Eu by Mn-oxide minerals and organo-metal colloids, and advective transport of these phases are responsible for the observed positive Eu anomalies in the JRB-CZO study site.

4.3.3. Processes that favor Y/Ho fractionation

Different behaviors of yttrium and holmium, which exhibit nearly identical ionic radii and charge, have been used to characterize the importance of complexing agents and neo-formed (oxy)hydroxide precipitates in weathering processes (Thompson et al., 2013). The

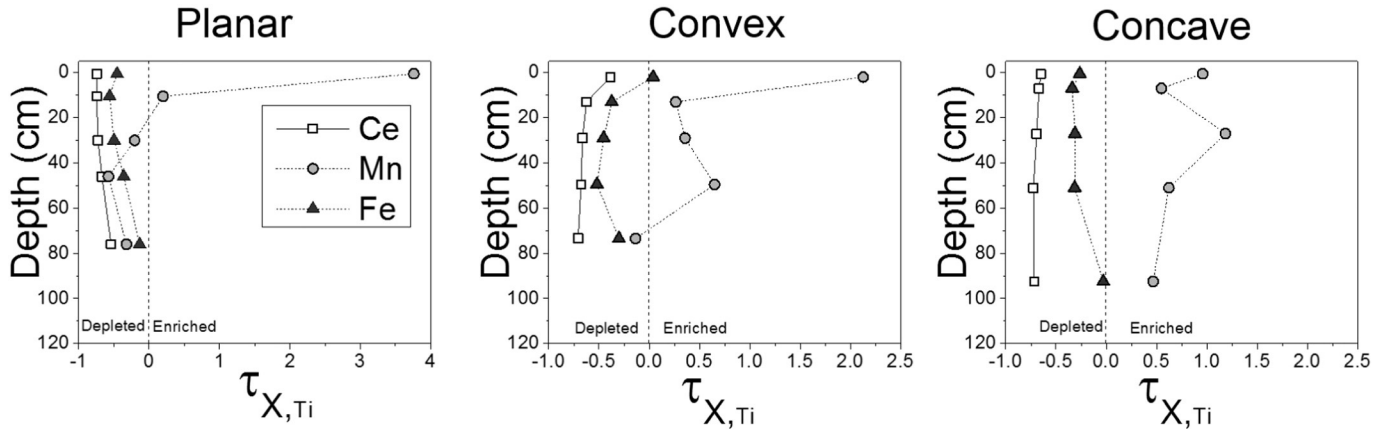

Fig. 11. Mass balance (tau) plots for Ce, Mn, and Fe as a function of depth for the planar, convex and concave hillslope profiles. Titanium was used as the immobile element. All values were normalized by the weighted average of ZOB bedrock concentrations. Tau values higher (lower) than 0 represent enrichment (depletion) relative to the parent materials.

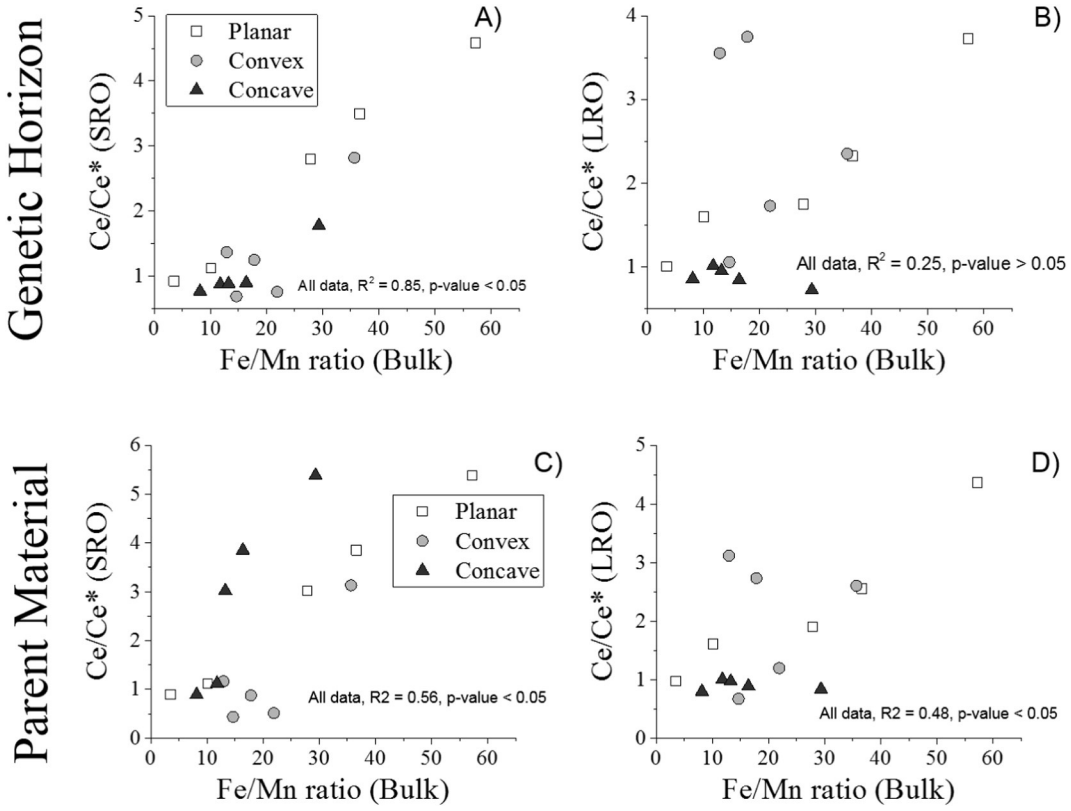

Fig. 12. Comparison between (A) Ce/Ce* (SRO) and (B) Ce/Ce* (LRO) normalized to the genetic horizon versus Fe/Mn ratios obtained from the bulk soil. Also, comparison between (C) Ce/Ce* (SRO) and (D) Ce/Ce* (LRO) normalized to the parent materials versus Fe/Mn ratios obtained from the bulk soil.

outer electron structure of Y^{3+}, comprising an empty 4f electron shell, induces a lower polarizability (lower propensity for electron field distortion) and a diminished tendency to form covalent metal–ligand bonds with organic acids and secondary minerals (Peppard et al., 1969; Byrne and Lee, 1993; Bau, 1999; Bau and Koschinsky, 2009; Thompson et al., 2013). This leads to the potential for divergent Y/Ho fractionation behavior during secondary mineral formation. Exclusion of Y (relative to Ho) during precipitation of secondary Fe(III)-(oxy)hydroxides in soils has been previously reported (Thompson et al., 2013). Measurement of Y/Ho fractionation during pedogenesis could therefore be useful for interpreting associated incongruent weathering processes.

The SE data reported here reveal that, in most instances, the Fe-oxides (SRO and LRO) in all pedons were relatively depleted in Y with a coherent decrease in Y/Ho ratios as a function of depth (Fig. 8D and E). The Y/Ho ratios reflect differential incorporation of these elements in pedogenic Fe-(oxy)hydroxide precipitates. In the planar location, negative associations between Y/Ho ratios (SRO and LRO) normalized to the genetic horizons and Fe:Mn ratios (bulk soil) were observed (SRO: $R^2 = 0.69$, p-value > 0.05; LRO: $R^2 = 0.92$, p-value < 0.05) (Table 3 and Fig. 13), indicating the exclusion of Y in the Fe-oxides. Also, a negative correlation between Y/Ho ratios (SRO) and Fe:Mn ratio (bulk soil) ($R^2 = 0.37$, p-value < 0.05) including all data normalized by the parent materials was observed (Table 3). LRO Fe-oxides, such as goethite, are more abundant than SRO Fe-oxides, such as ferrihydrite (Fig. A.4, Appendix), and the former are more depleted in Y (Fig. 8E). As solid-state transformation and ripening occurs in the Fe-oxides, REY are expelled from the structure and subjected to increasing depletion (Laveuf and Cornu, 2009), and such an effect therefore appears escalated for Y. Our results are in agreement with those of Thompson et al. (2013), who showed that Y exhibits a low affinity for secondary Fe-(oxy)hydroxide minerals precipitating during weathering of Hawaiian basalt. Mn-oxides in our study site were significantly more enriched in Y than was the total solid phase, indicating the importance of Mn-oxides to Y sequestration, with a larger enrichment in the upper horizons (Fig. 8B). In the planar location, a positive correlation between Y/Ho ratios and Mn concentrations in the Mn-oxide extractable pool was observed ($R^2 = 0.91$, p-value < 0.05) (Table 3 and Fig. 13). In the concave location, a negative correlation between Y/Ho ratios obtained from the Mn-oxide pool and Fe:Mn ratio (bulk soil) was observed ($R^2 = 0.85$, p-value < 0.05) (Table 3 and Fig. 13). Also, a positive correlation between Y/Ho ratios and Mn concentrations in the Mn-oxide extractable pool ($R^2 = 0.39$, p-value < 0.05) including all data normalized by the parent materials was observed (Table 3). Likewise, Bau and Koschinsky (2009) reported Lu-normalized mineral/seawater ratios for Mn- and Fe-oxides ($K_D^{REY\text{-}oxide/REY\text{-}sw}{}_{Lu}$ and concluded that Y was more depleted in the Fe-oxides than in the Mn-oxides. Furthermore, among all pools targeted in the SE (with the exception of the residual pool), a large mass fraction of both Y and Ho was associated with the organo-metal colloid pool (especially in the convex site), suggesting that these organo-mineral weathering products play an important role in Y and Ho transport and fate in these soils (Fig. A.5, Appendix).

5. Summary and conclusions

The detailed study of weathering profiles located in planar, convex and concave landscape positions indicates that, in addition to pedon depth, landscape position plays a significant role in the accumulation and depletion of distinct REY weathering products. The REY signatures in soils are influenced not only by depth-dependent variation in water and dissolved organic carbon (DOC) fluxes, but also by multiple competing biogeochemical weathering processes (e.g. aqueous complexation, solid-solution partitioning, incongruent mineral formation).

In the concave site, pedogenic REY fractionation was accompanied by coherent and statistically significant ($p < 0.05$) decreases in the extent of depletion (removal) of REY with distance from saprock to

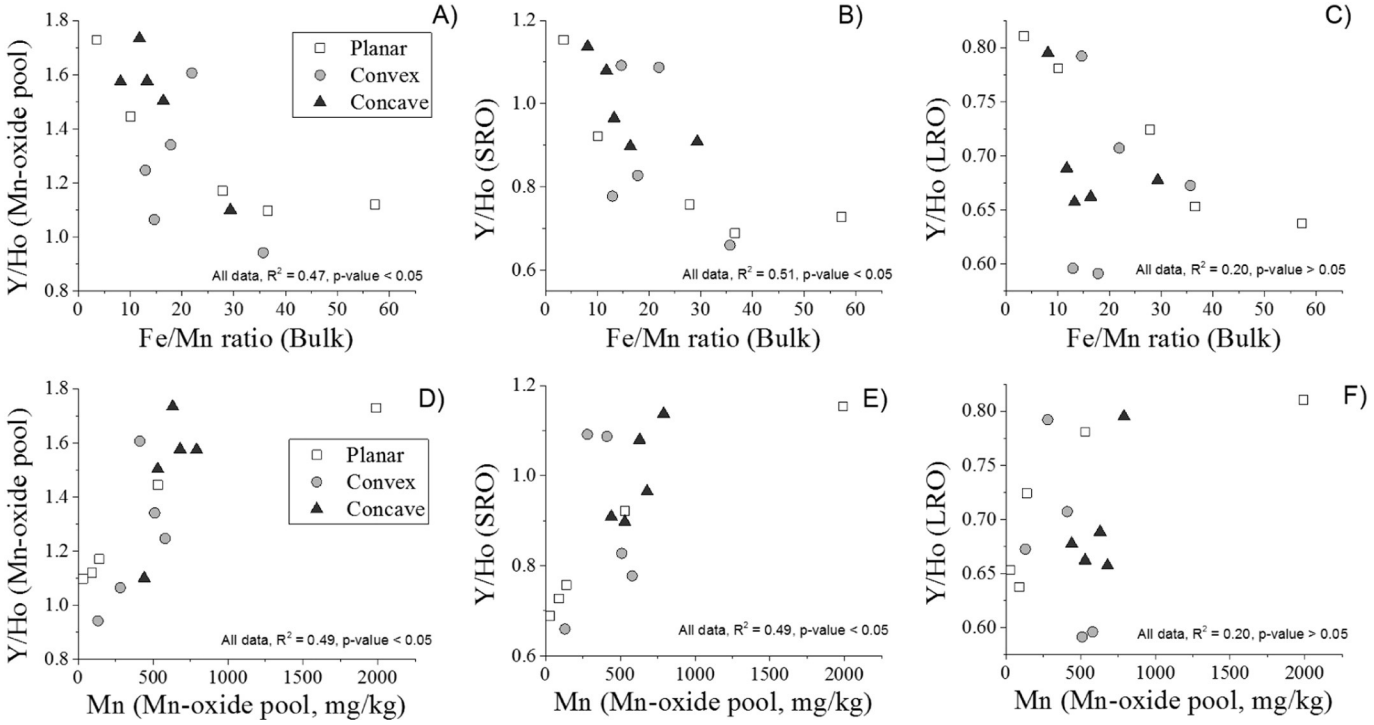

Fig. 13. Comparison between (A) Y/Ho (Mn-oxide pool), (B) Y/Ho (SRO), and (C) Y/Ho (LRO) normalized to the genetic horizon versus Fe/Mn ratios obtained from the bulk soil. Also, comparison between (D) Y/Ho (Mn-oxide pool), (E) Y/Ho (SRO), and (F) Y/Ho (LRO) normalized to the genetic horizon versus Mn concentrations obtained from the Mn-oxide pool.

surface — a trend that is distinct from the inverse trend often reported for pedons subjected to dominantly 1D hydrologic (vertical) downward flux (e.g., ridgetop or divergent sites). This result was, however, consistent with the relatively higher water and organic C through fluxes measured at depth for the concave site, indicating that it results from the long-term influence of subsurface hydrologic flows passing laterally over less permeable saprock. More typical trends (increased REY depletion with distance from saprock to surface) were observed in the planar profile ($p < 0.05$), which was evidently not subjected to large lateral subsidies of water and organic carbon flux.

Despite high variation in REY patterns as a function of landscape position and pedon depth, distinct steps of a sequential extraction scheme extract internally consistent REY patterns across all soil samples. Notable, for example, is the enrichment of MREE in organo-mineral weathering products, and relative MREE depletion in residual primary minerals and silicates. Hence, the overarching effect of incongruent weathering in the CZO soils appears to be translocation of MREE from parent minerals into secondary organo-mineral forms, whereas LREE, are preferentially removed from the soil profile. Among the secondary phases quantified, dispersible organo-metal colloids consistently comprised the largest pool of MREE, indicating that conditions favoring colloidal transport (e.g., soil saturation) and prolonged reducing conditions, could mobilize MREE and DOM into receiving waters. REY enrichment in the upper horizons of the convex profile are consistent with lateral colluvial transport of REY–organic complexes from upslope.

Strongly positive Ce anomalies were revealed during reductive dissolution of Fe-oxides, and the anomalies were observed to increase systematically with depth in the planar site, consistent with preferential accumulation of Ce in reducible ferric (oxy)hydroxide solids. In the planar profile, redox conditions and incongruent mineral formation are likely controlling the down-profile accumulation of Ce. The systematically low Y/Ho ratios in SRO and LRO Fe(III)-oxide pools reflects the exclusion of Y relative to Ho during nucleation and growth of these pedogenic precipitates.

The exchange complex exhibited large positive Eu anomalies, particularly in surface soils, indicating that Eu contributes disproportionately to the Na-acetate exchangeable REY pool. Surface soils also contained a large pool (positive anomaly) of Eu that was released with reducible Mn oxides. Preferential sequestration of Eu by adsorption to surfaces and coprecipitation with reducible Mn oxides, along with a large mass fraction of Eu associated with the organo-metal complexes and dispersible colloids evidently explains the overall enrichment of Eu in the bulk soil matrix reported previously (Vázquez-Ortega et al., 2015).

Taken together, results of this work indicate that REY signatures are useful in signaling biogeochemical processes controlling organo-metal colloid mobilization. MREE mobilization to surface waters would therefore also signal de-stabilization of an important pool of mineral-associated OM, whereas positive Ce anomalies in drainage waters could signal reductive dissolution of Fe(III)-(oxy)hydroxides.

Acknowledgments

The Catalina-Jemez Critical Zone Observatory is supported by the National Science Foundation, Grant no. EAR-1331408. Thanks to Juliana Gil, Mark Losleben, Scott Compton, Caitlin Orem, and Mercer Meding for assistance with sampling and analysis.

Appendix A. Supplementary data

Supplementary data to this article can be found online at http://dx.doi.org/10.1016/j.chemgeo.2016.01.001.

References

Anders, E., Grevesse, N., 1989. Abundances of the elements — meteoritic and solar. Geochim. Cosmochim. Acta 53, 197–214.

Aubert, D., Stille, P., Probst, A., 2001. REE fractionation during granite weathering and removal by waters and suspended loads: Sr and Nd isotopic evidence. Geochim. Cosmochim. Acta 65, 387–406.

Aubert, D., Stille, P., Probst, A., Gauthier-Lafaye, F., Pourcelot, L., Del Nero, M., 2002. Characterization and migration of atmospheric REE in soils and surface waters. Geochim. Cosmochim. Acta 66, 3339–3350.

Bau, M., 1999. Scavenging of dissolved yttrium and rare earths by precipitating iron oxyhydroxide: experimental evidence for Ce oxidation, Y–Ho fractionation, and lanthanide tetrad effect. Geochim. Cosmochim. Acta 63, 67–77.

Bau, M., Koschinsky, A., 2009. Oxidative scavenging of cerium on hydrous Fe oxide: evidence from the distribution of rare earth elements and yttrium between Fe oxides and Mn oxides in hydrogenetic ferromanganese crusts. Geochem. J. 43, 37–47.

Bau, M., Dulski, P., Moller, P., 1995. Yttrium and holmium in south-Pacific seawater — vertical-distribution and possible fractionation mechanisms. Chem. Erde-Geochem. 55, 1–16.

Beven, K.J., Kirkby, M.J., 1979. A physically based, variable contributing area model of basin hydrology. Hydrol. Sci. Bull. 24, 43–69.

Biddle, D.L., Chittleborough, D.J., Fitzpatrick, R.W., 1995. Field monitoring of solute and colloid mobility in a gneissic sub-catchment, South Australia. Appl. Clay Sci. 9, 433–442.

Braun, J., Pagel, M., Muller, J., Bilong, P., Michard, A., Guillet, B., 1990. Cerium anomalies in lateritic profiles. Geochim. Cosmochim. Acta 54, 781–795.

Braun, J., Pagel, M., Herbillon, A., Rosin, C., 1993. Mobilization and redistribution of REEs and thorium in a syenitic lateritic profile — a mass-balance study. Geochim. Cosmochim. Acta 57, 4419–4434.

Braun, J., Viers, J., Dupre, B., Polve, M., Ndam, J., Muller, J.P., 1998. Solid/liquid REE fractionation in the lateritic system of Goyoum, east Cameroon: the implication for the present dynamics of the soil covers of the humid tropical regions. Geochim. Cosmochim. Acta 62, 273–299.

Brioschi, L., Steinmann, M., Lucot, E., Pierret, M.C., Stille, P., Prunier, J., Badot, P.M., 2013. Transfer of rare earth elements (REE) from natural soil to plant systems: implications for the environmental availability of anthropogenic REE. Plant Soil 366, 143–163.

Brooks, P.D., Vivoni, E.R., 2008. Mountain ecohydrology: quantifying the role of vegetation in the water balance of montane catchments. Ecohydrology 1, 187–192.

Byrne, R., Lee, J., 1993. Comparative yttrium and rare-earth element chemistries in seawater. Mar. Chem. 44, 121–130.

Byrne, R., Li, B., 1995. Comparative complexation behavior of the rare-earths. Geochim. Cosmochim. Acta 59, 4575–4589.

Chadwick, O.A., Brimhall, G.H., Hendricks, D.M., 1990. From a black to a gray box — a mass balance interpretation of pedogenesis. Geomorphology 3, 369–390.

Chadwick, O., Derry, L., Vitousek, P., Huebert, B., Hedin, L., 1999. Changing sources of nutrients during four million years of ecosystem development. Nature 397, 491–497.

Chipera, S.J., Goff, F., Goff, C.J., Fittipaldo, M., 2008. Zeolitization of intracaldera sediments and rhyolitic rocks in the 1.25 Ma lake of Valles caldera, New Mexico, USA. J. Volcanol. Geotherm. Res. 178, 317–330.

Chorover, J., Troch, P.A., Rasmussen, C., Brooks, P.D., Pelletier, J.D., Breshars, D.D., Huxman, T.E., Kurc, S.A., Lohse, K.A., McIntosh, J.C., Meixner, T., Schaap, M.G., Litvak, M.E., Perdrial, J., Harpold, A., Durcik, M., 2011. How water, carbon, and energy drive critical zone evolution: the Jemez-Santa Catalina Critical Zone Observatory. Vadose Zone J. 10, 884–899.

Coppin, F., Berger, G., Bauer, A., Castet, S., Loubet, M., 2002. Sorption of lanthanides on smectite and kaolinite. Chem. Geol. 182, 57–68.

Cullers, R., Chaudhuri, S., Arnold, B., Lee, M., Wolf, C., 1975. Rare-earth distributions in clay-minerals and in clay-sized fraction of Lower Permian Havensville and Eskridge shales of Kansas and Oklahoma. Geochim. Cosmochim. Acta 39, 1691–1703.

Davranche, M., Pourret, O., Gruau, G., Dia, A., 2004. Impact of humate complexation on the adsorption of REE onto Fe oxyhydroxide. J. Colloid Interface Sci. 277, 271–279.

Davranche, M., Pourret, O., Gruau, G., Dia, A., Le Coz-Bouhnik, M., 2005. Adsorption of REE(III)–humate complexes onto MnO_2: experimental evidence for cerium anomaly and lanthanide tetrad effect suppression. Geochim. Cosmochim. Acta 69, 4825–4835.

Davranche, M., Grybos, M., Gruau, G., Pedrot, M., Dia, A., Marsac, R., 2011. Rare earth element patterns: a tool for identifying trace metal sources during wetland soil reduction. Chem. Geol. 284, 127–137.

De Carlo, E., Wen, X., 1998. The influence of redox reactions on the uptake of dissolved Ce by suspended Fe and Mn oxide particles. Aquat. Geochem. 3, 357–389.

DeBaar, H., German, C., Elderfield, H., Vangaans, P., 1988. Rare-earth element distributions in anoxic waters of the Cariaco Trench. Geochim. Cosmochim. Acta 52, 1203–1219.

Douville, E., Bienvenu, P., Charlou, J., Donval, J., Fouquet, Y., Appriou, P., Gamo, T., 1999. Yttrium and rare earth elements in fluids from various deep-sea hydrothermal systems. Geochim. Cosmochim. Acta 63, 627–643.

Elderfield, H., 1988. The oceanic chemistry of the rare-earth elements. Philos. Trans. R. Soc. A Math. Phys. Eng. Sci. 325, 105–126.

Elderfield, H., Upstillgoddard, R., Sholkovitz, E., 1990. The rare-earth elements in rivers, estuaries, and coastal seas and their significance to the composition of ocean waters. Geochim. Cosmochim. Acta 54, 971–991.

Evensen, N., Hamilton, P., Onions, R., 1978. Rare-earth abundances in chondritic meteorites. Geochim. Cosmochim. Acta 42, 1199–1212.

Feng, J., 2010. Behaviour of rare earth elements and yttrium in ferromanganese concretions, gibbsite spots, and the surrounding terra rossa over dolomite during chemical weathering. Chem. Geol. 271, 112–132.

Gangloff, S., Stille, P., Pierret, M., Weber, T., Chabaux, F., 2014. Characterization and evolution of dissolved organic matter in acidic forest soil and its impact on the mobility of major and trace elements (case of the Strengbach watershed). Geochim. Cosmochim. Acta 130, 21–41.

Goff, F., Gardner, J., 1988. Valles Caldera region, New Mexico, and the emerging continental scientific drilling program. J. Geophys. Res. Solid Earth Planets 93, 5997–5999.

Goldberg, E., Smith, R., Koide, M., Schmitt, R., 1963. Rare-earth distributions in marine environment. J. Geophys. Res. 68, 4209–4217.

Goyne, K.W., Brantley, S.L., Chorover, J., 2010. Rare earth element release from phosphate minerals in the presence of organic acids. Chem. Geol. 278, 1–14.

Guo, Q., Pelletier, J., Parmenter, R., Allen, C., Judy, B., Durcik, M., 2010a. CZO Dataset: Jemez River Basin — LiDAR (2010) — Snow-off. Accessed from http://criticalzone.org/catalina-jemez/data/dataset/2613/.

Guo, H., Zhang, B., Wang, G., Shen, Z., 2010b. Geochemical controls on arsenic and rare earth elements approximately along a groundwater flow path in the shallow aquifer of the HetaoBasin, Inner Mongolia. Chem. Geol. 270, 117–125.

Holder, M., Brown, K., Thomas, J., Zabcik, D., Murray, H., 1991. Capillary-wick unsaturated zone soil pore water sampler. Soil Sci. Soc. Am. J. 55, 1195–1202.

Huckle, D., Ma, L., McIntosh, J., Rasmussen, C., Vázquez-Ortega, A., Chorover, J., 2016. U-series isotopic signatures of soils and headwater streams in a semi-arid complex volcanic terrain. Chem. Geol. (submitted for publication).

Johannesson, K., Stetzenbach, K., Hodge, V., 1997. Rare earth elements as geochemical tracers of regional groundwater mixing. Geochim. Cosmochim. Acta 61, 3605–3618.

Johannesson, K., Tang, J., Daniels, J., Bounds, W., Burdige, D., 2004. Rare earth element concentrations and speciation in organic-rich blackwaters of the Great Dismal Swamp, Virginia, USA. Chem. Geol. 209, 271–294.

Johannesson, K.H., Telfeyan, K., Chevis, D.A., Rosenheim, B.E., Leybourne, M.I., Furnes, H., 2014. Rare earth elements in stromatolites — 1. Evidence that modern terrestrial stromatolites fractionate rare earth elements during incorporation from ambient waters. In: Dilek, Y. (Ed.), Evolution of Archean Crust and Early Life. Springer, Dordrecht, pp. 385–411.

Kurtz, A., Derry, L., Chadwick, O., 2001. Accretion of Asian dust to Hawaiian soils: isotopic, elemental, and mineral mass balances. Geochim. Cosmochim. Acta 65, 1971–1983.

Land, M., Ohlander, B., Ingri, J., Thunberg, J., 1999. Solid speciation and fractionation of rare earth elements in a spodosol profile from northern Sweden as revealed by sequential extraction. Chem. Geol. 160, 121–138.

Laveuf, C., Cornu, S., 2009. A review on the potentiality of rare earth elements to trace pedogenetic processes. Geoderma 154, 1–12.

Laveuf, C., Cornu, S., Juillot, F., 2008. Rare earth elements as tracers of pedogenetic processes. Compt. Rendus Geosci. 340, 523–532.

Laveuf, C., Cornu, S., Guilherme, L.R.G., Guerin, A., Juillot, F., 2012. The impact of redox conditions on the rare earth element signature of redoximorphic features in a soil sequence developed from limestone. Geoderma 170, 25–38.

Leybourne, M.I., Johannesson, K.H., 2008. Rare earth elements (REE) and yttrium in stream waters, stream sediments, and Fe-Mn oxyhydroxides: fractionation, speciation, and controls over REE plus Y patterns in the surface environment RID B-2541-2009. Geochim. Cosmochim. Acta 72, 5962–5983.

Ma, L., Jin, L., Brantley, S.L., 2011. How mineralogy and slope aspect affect REE release and fractionation during shale weathering in the Susquehanna/Shale Hills Critical Zone Observatory. Chem. Geol. 290, 31–49.

Marsac, R., Davranche, M., Gruau, G., Dia, A., Bouhnik-Le Coz, M., 2012. Aluminium competitive effect on rare earth elements binding to humic acid. Geochim. Cosmochim. Acta 89, 1–9.

Marsac, R., et al., 2013. Effects of Fe competition on REE binding to humic acid: origin of REE pattern variability in organic waters. Chem. Geol. 342, 119–127.

Mikutta, R., Baumgaertner, A., Schippers, A., Haumaier, L., Guggenberger, G., 2012. Extracellular polymeric substances from Bacillus subtilis associated with minerals modify the extent and rate of heavy metal sorption. Environ. Sci. Technol. 46, 3866–3873.

Moore, I.D., Grayson, R.B., Ladson, A.R., 1991. Digital terrain modelling: a review of hydrological, geomorphological, and biological applications. Hydrol. Process. 5, 3–30.

Nakajima, T., Terakado, Y., 2003. Rare earth elements in stream waters from the Rokko granite area, Japan: effect of weathering degree of watershed rocks. Geochem. J. 37, 181–198.

Nezat, C.A., Blum, J.D., Yanai, R.D., Hamburg, S.P., 2007. A sequential extraction to determine the distribution of apatite in granitoid soil mineral pools with application to weathering at the Hubbard Brook Experimental Forest, NH, USA. Appl. Geochem. 22, 2406–2421.

NRC, 2001. Basic Research Opportunities in Earth Sciences. National Academies Press, Washington, DC, National Research Council.

Ohta, A., Kawabe, I., 2001. REE(III) adsorption onto Mn dioxide (delta-MnO_2) and Fe oxyhydroxide: Ce(III) oxidation by delta-MnO_2. Geochim. Cosmochim. Acta 65, 695–703.

Panahi, A., Young, G., Rainbird, R., 2000. Behavior of major and trace elements (including REE) during Paleoproterozoic pedogenesis and diagenetic alteration of an Archean granite near Ville Marie, Quebec, Canada. Geochim. Cosmochim. Acta 64, 2199–2220.

Peppard, D., Mason, G., Lewey, S., 1969. A tetrad effect in liquid–liquid extraction ordering of lanthanides (3). J. Inorg. Nucl. Chem. 31, 2271–2272.

Perdrial, J.N., Perdrial, N., Harpold, A., Gao, X., Gabor, R., LaSharr, K., Chorover, J., 2012. Impacts of sampling dissolved organic matter with passive capillary wicks versus aqueous soil extraction. Soil Sci. Soc. Am. J. 76, 2019–2030.

Perdrial, J.N., McIntosh, J., Harpold, A., Brooks, P.D., Zapata-Rios, X., Ray, J., Meixner, T., Kanduc, T., Litvak, M., Troch, P.A., Chorover, J., 2014a. Stream water carbon controls in seasonally snow-covered mountain catchments: impact of inter-annual variability of water fluxes, catchment aspect and seasonal processes. Biogeochemistry 118, 273–290.

Perdrial, J.N., Perdrial, N., Vazquez-Ortega, A., Porter, C., Leedy, J., Chorover, J., 2014b. Experimental assessment of passive capillary wick sampler suitability for inorganic soil solution constituents. Soil Sci. Soc. Am. J. 78, 486–495.

Pokrovsky, O., Schott, J., 2002. Iron colloids/organic matter associated transport of major and trace elements in small boreal rivers and their estuaries (NW Russia). Chem. Geol. 190, 141–179.

Porder, S., Hilley, G.E., Chadwick, O.A., 2007. Chemical weathering, mass loss, and dust inputs across a climate by time matrix in the Hawaiian Islands. Earth Planet. Sci. Lett. 258, 414–427.

Pourret, O., Martinez, R.E., 2009. Modeling lanthanide series binding sites on humic acid. J. Colloid Interface Sci. 330, 45–50.
Pourret, O., Davranche, M., Gruau, G., Dia, A., 2007a. Organic complexation of rare earth elements in natural waters: evaluating model calculations from ultrafiltration data. Geochim. Cosmochim. Acta 71, 2718–2735.
Pourret, O., Davranche, M., Gruau, G., Dia, A., 2007b. Rare earth elements complexation with humic acid. Chem. Geol. 243, 128–141.
Pourret, O., Gruau, G., A, D., Davranche, M., Molenat, J., 2010. Colloidal control on the distribution of rare earth elements in shallow groundwaters. Aquat. Geochem. 16, 31–59.
Ronov, A., Balashov, Y., Migdisov, A., 1967. Geochemistry of rare earths in sedimentary cycle. Geochem. Int. USSR 4, 1–10.
Schijf, J., Byrne, R., 2001. Stability constants for mono- and dioxalato-complexes of Y and the REE, potentially important species in groundwaters and surface freshwaters. Geochim. Cosmochim. Acta 65, 1037–1046.
Shiller, A.M., 2010. Dissolved rare earth elements in a seasonally snow-covered, alpine/subalpine watershed, Loch Vale, Colorado. Geochim. Cosmochim. Acta 74, 2040–2052.
Sholkovitz, E., 1992. Chemical evolution of rare-earth elements — fractionation between colloidal and solution phases of filtered river water. Earth Planet. Sci. Lett. 114, 77–84.
Sonke, J.E., Salters, V.J.M., 2006. Lanthanide–humic substances complexation, I. Experimental evidence for a lanthanide contraction effect. Geochim. Cosmochim. Acta 70, 1495–1506.
Steinmann, M., Stille, P., 2006. Rare earth element transport and fractionation in small streams of a mixed basaltic-granitic catchment basin (Massif Central, France). J. Geochem. Explor. 88, 336–340.
Steinmann, M., Stille, P., 2008. Controls on transport and fractionation of the rare earth elements in stream water of a mixed basaltic–granitic catchment basin (Massif Central, France). Chem. Geol. 254, 1–18.
Stille, P., Steinmann, M., Pierret, M., Gauthier-Lafaye, F., Aubert, D., Probst, A., Viville, D., Chabaux, F., 2006a. The impact of vegetation on fractionation of rare earth elements (REE) during water–rock interaction. J. Geochem. Explor. 88, 341–344.
Stille, P., Steinmann, M., Pierret, M., Gauthier-Lafaye, F., Chabaux, F., Viville, D., Pourcelot, L., Matera, V., Aouad, G., Aubert, D., 2006b. The impact of vegetation on REE fractionation in stream waters of a small forested catchment (the Strengbach case). Geochim. Cosmochim. Acta 70, 3217–3230.
Stille, P., Pierret, M., Steinmann, M., Chabaux, F., Boutin, R., Aubert, D., Pourcelot, L., Morvan, G., 2009. Impact of atmospheric deposition, biogeochemical cycling and water–mineral interaction on REE fractionation in acidic surface soils and soil water (the Strengbach case). Chem. Geol. 264, 173–186.
Tang, J., Johannesson, K., 2003. Speciation of rare earth elements in natural terrestrial waters: assessing the role of dissolved organic matter from the modeling approach. Geochim. Cosmochim. Acta 67, 2321–2339.
Tang, J., Johannesson, K.H., 2010a. Ligand extraction of rare earth elements from aquifer sediments: implications for rare earth element complexation with organic matter in natural waters. Geochim. Cosmochim. Acta 74, 6690–6705.
Tang, J., Johannesson, K.H., 2010b. Rare earth elements adsorption onto Carrizo sand: influence of strong solution complexation. Chem. Geol. 279, 120–133.
Tarboton, D.G., 1997. A new method for the determination of flow directions and upslope areas in grid digital elevation models. Water Resour. Res. 33, 309–319.
Taylor, S., McLennan, S., 1981. The composition and evolution of the continental-crust — rare-earth element evidence from sedimentary-rocks. Philos. Trans. R. Soc. London, Ser. A 301, 381–399.
Thompson, A., Chadwick, O.A., Boman, S., Chorover, J., 2006. Colloid mobilization during soil iron redox oscillations. Environ. Sci. Technol. 40, 5743–5749.
Thompson, A., Amistadi, M.K., Chadwick, O.A., Chorover, J., 2013. Fractionation of yttrium and holmium during basaltic soil weathering. Geochim. Cosmochim. Acta 119, 18–30.
Torn, M.S., Trumbore, S.E., Chadwick, O.A., Votousek, P.M., Hendricks, D.M., 1997. Mineral control of soil organic carbon storage and turnover. Nature 389, 170–173.
Vázquez-Ortega, A., Hernandez-Ruiz, S., Amistadi, M.K., Rasmussen, C., Chorover, J., 2014. Fractionation of dissolved organic matter by (oxy)hydroxide-coated sands: competitive sorbate displacement during reactive transport. Vadose Zone J. 13, 1–13.
Vázquez-Ortega, A., Perdrial, J.N., Harpold, A., Zapata-Rios, X., Rasmussen, C., McIntosh, J., Schaap, M., Pelletier, J., Brooks, P., Amistadi, M.K., Chorover, J., 2015. Rare earth elements as reactive tracers of biogeochemical weathering in forested rhyolitic terrain. Chem. Geol. 391, 19–32.
Viers, J., Dupre, B., Polve, M., Schott, J., Dandurand, J., Braun, J., 1997. Chemical weathering in the drainage basin of a tropical watershed (Nsimi-Zoetele site, Cameroon): comparison between organic-poor and organic-rich waters. Chem. Geol. 140, 181–206.
Weill, D., Drake, M., 1973. Europium anomaly in plagioclase feldspar — experimental results and semiquantitative model. Science 180, 1059–1060.
Willis, S.S., Johannesson, K.H., 2011. Controls on the geochemistry of rare earth elements in sediments and groundwaters of the Aquia aquifer, Maryland, USA. Chem. Geol. 285, 32–49.
Wood, S.A., 1990. The aqueous geochemistry of the rare-earth elements and yttrium: 1. Review of available low-temperature data for inorganic complexes and the inorganic REE speciation of natural waters. Chem. Geol. 82, 159–186.
Xiong, Y., 2011. Organic species of lanthanum in natural environments: implications to mobility of rare earth elements in low temperature environments. Appl. Geochem. 26, 1130–1137.
Yamamoto, Y., Takahashi, Y., Shimizu, H., 2005. Systematics of stability constants of fulvate complexes with rare earth ions. Chem. Lett. 34, 880–881.
Yamamoto, Y., Takahashi, Y., Shimizu, H., 2010. Systematic change in relative stabilities of REE–humic complexes at various metal loading levels. Geochem. J. 44, 39–63.
Zevenbergen, L.W., Thorne, C.R., 1987. Quantitative analysis of land surface topography. Earth Surf. Process. Landf. 12, 47–56.